Journal of Visualized Experiments

Macro-rheology characterization of gill raker mucus in the Silver Carp, Hypophthalmichthys molitrix

--Manuscript Draft--

Article Type:	Methods Article - JoVE Produced Video
Manuscript Number:	JoVE61379R3
Full Title:	Macro-rheology characterization of gill raker mucus in the Silver Carp, Hypophthalmichthys molitrix
Section/Category:	JoVE Engineering
Keywords:	Silver carp Mucus Rheology Filter feeding Rheometry Biological fluids Hydrogels
Corresponding Author:	Kartik Venkat Bulusu, D.Sc. George Washington University Washington DC, District of Columbia UNITED STATES
Corresponding Author's Institution:	George Washington University
Corresponding Author E-Mail:	bulusu@gwu.edu
Order of Authors:	Kartik Venkat Bulusu, D.Sc.
	Samantha Racan
	Michael W. Plesniak
Additional Information:	
Question	**Response**
Please indicate whether this article will be Standard Access or Open Access.	Standard Access (US$2,400)
Please indicate the **city, state/province, and country** where this article will be **filmed**. Please do not use abbreviations.	Washington DC

Powered by Editorial Manager® and ProduXion Manager® from Aries Systems Corporation

Manuscript Click here to access/download;Manuscript;61379_R3_RE.docx

TITLE:

Macro-Rheology Characterization of Gill Raker Mucus in the Silver Carp, *Hypophthalmichthys molitrix*

AUTHORS AND AFFILIATIONS:

Kartik V. Bulusu[1], Samantha Racan[1], Michael W. Plesniak[1]

[1]Department of Mechanical and Aerospace Engineering, The George Washington University, Washington DC, USA

Corresponding author:
Kartik V. Bulusu (bulusu@gwu.edu)

Email Addresses of Co-Authors:
Samantha Racan (samracan19@gwu.edu)
Michael W. Plesniak (plesniak@gwu.edu)

KEYWORDS

silver carp, mucus, rheology, filter feeding, rheometry, biological fluids, hydrogels

SUMMARY

This protocol presents a method to perform rheology characterization of mucus that resides on gill rakers (GR) of the silver carp. Viscoelastic characteristics of GR-mucus, obtained by measuring viscosity, storage and loss moduli, are evaluated for the apparent yield stress to understand the filter feeding mechanism in GR.

ABSTRACT

The silver carp, *Hypophthalmichthys molitrix*, is an invasive planktivorous filter feeder fish that infested the natural waterways of the upper Mississippi River basin due to their highly efficient filter feeding mechanism. The characteristic organs called gill rakers (GRs), found in many such filter feeders, facilitate the efficient filtration of food particles such as phytoplankton that are of a few microns in size.

The motivation to investigate the rheology of the GR mucus arose from its potential to aid the filter feeding process in the silver carp. Based on this it was hypothesized that GR mucus may provide an adhesive function to food particles and act as a transport vehicle to assist in the filter feeding process. The mucus-rich fluid that is in a 'thick and sticky' state may facilitate the adhesion of food particulates. The permeation and transport through the GR membrane are facilitated by the action of external shear forces that induce varying shear strain rates. Therefore, mucus rheology can provide a vital clue to the tremendous outcompeting nature of the silver carp within the pool of filter feeding fish.

The main objective of the protocol is to the determine the yield stress of the mucus, attributed to the minimum shear stress required to initiate flow at which irreversible plastic deformation is

first observed across a structured viscoelastic material. Accordingly, rheological properties of the GR mucus, i.e., viscosity, storage, and loss moduli, were investigated for its non-Newtonian, shear-thinning nature using a rheometer.

A protocol presented here analyzes the rheological properties of mucus extracted from the gill rakers of a silver carp, fished at Hart Creek location of the Missouri River. The protocol aims to develop an effective strategy for rheological testing and material characterization of mucus (assumed to be a structured viscoelastic material) acquired from silver carp.

INTRODUCTION

The silver carp, *Hypophthalmichthys molitrix*, is a planktivorous filter feeder and an invasive species that has infiltrated several natural waterways in the United States. This species was initially introduced in the upper Mississippi River basin to control algal blooms[1-3]. The silver carp is an extremely efficient feeder. Typically, its consumable food particle sizes range from 4 to 20 µm to larger zooplankton that are around 80 µm[3-5]. This species has outcompeted other native fish and can potentially cause enormous damage to native waterways by limiting available resources[1-2,6]. Thus, filter feeding fish such as the silver carp and the bighead carp pose a major threat to the Great Lakes[1-2,6-8].

Filter feeding fish possess special organs called the gill rakers (GRs) with a thin layer of mucus residing on their surface. These organs improve the efficiency of filtration and aggregation of small particles from the incoming fluid. The goal of the protocol presented herein is to characterize the non-Newtonian, shear thinning material property and yield stress of the GR mucus acquired from the inner surface of the gill rakers in the silver carp. The value of yield stress of the GR-mucus, ascertained using a rotational rheometer, is of interest. The measured yield stress is referred to as an "apparent yield stress" since it depends on the testing methods such as steady shear rate- or dynamic oscillatory strain-type[9-10]. Currently the most utilized rheological phenomenon is the shear-thinning 'yield-stress fluid,' or the transition from solid-like to liquid-like behavior at a critical applied stress[9,11]. The apparent yield stress is the minimum shear stress required to initiate flow or that at which irreversible plastic deformation is first observed when the mucus transitions from a gel-like material to a fluid-like material. This behavior can be observed in structured viscoelastic materials such as the mucus layer on GRs. The transition from gel-like to fluid-like behavior of the GR mucus entails two functions i.e., an adhesive role to gather food particulates and a transport vehicle role to assist in the delivery and filtration process. The extended function of the mucus includes creating diffusion barriers in disease resistance and respiration, providing controlled release of nutritional factors, toxic components and excretion, metabolic pathways for feeding and nesting, predator protection, and boundary layer modification that improves the locomotion and propulsive efficiency[12-14].

Complex fluids like the mucus possess properties that vary with flow conditions and require additional measurement parameters to define their bulk scale physical behavior. To monitor the viscosity and yield stress of GR mucus, rheological measurements are performed using a rotational rheometer. The rotational rheometer applies a steady or oscillatory shear stress or strain by means of a rotating disk in contact with the fluid sample and measures its response. The

rationale behind using this instrument and technique is that the rheometer can provide a set of measurements to describe the material properties of the GR mucus of the silver carp, which cannot be defined by viscosity alone.

The mucus is a viscoelastic material and its mechanical response to an imposed deformation is between that of a pure solid (governed by Hooke's law of elasticity) and that of a pure liquid (governed by Newton's law of viscosity)[15-16]. The complex macromolecular network contained within the mucus can stretch and reorient in response to external forces or deformation. A rotational rheometer is comprised of a cone geometry and a Peltier plate as shown in **Figure 1** and **Figure 2** (see **Table 1** for instrumentation specifications). The objective of this study was to develop a protocol to determine the rheological properties of the GR mucus. An advantage of the rotational rheometer over a viscometer is its ability to make dynamic measurements using small sample volumes. The GR mucus sample volume in this study was approximately 1.4 mL. The viscometer, on the other hand, is limited to constant shear rates and requires large sample volumes.

The rheological properties of the mucus are expected to vary greatly within the silver carp anatomy. For example, the rheological properties of the mucus residing on the inner GR surfaces may be different from that on the outer GR surfaces or the epibranchial organ. To account for the potential variability of mucus properties in different regions of the fish, the acquired GR mucus sample was diluted, and solutions of various concentrations were created to develop an understanding of the variation in rheology. The rotational rheometer with cone geometry and a Peltier plate was then used in this protocol to investigate the various small samples of mucus. The data and results regarding mucus rheology reported after executing the protocol demonstrated the efficacy of the measurement technique and were not meant to be generalized across the entire silver carp population. The protocol presented herein can be extended to investigate mucus rheology across larger sample sets to test other hypotheses.

The purpose of this study is to demonstrate the variation of rheological properties of GR mucus rheology with three different mucus concentrations (400 mg/mL, 200 mg/mL and 100 mg/mL). The 400 mg/mL concentration represents the raw mucus sample harvested from the fish GRs. Distilled water (DI) was used to dilute the raw mucus sample into 200 mg/mL and 100 mg/mL concentrations. Diluting the mucus samples allowed for the evaluation of the extent of shear thinning, apparent yield stress as a function of concentration and to determine the concentration at which the GR mucus transitions to non-Newtonian behavior. A shaker was used to break down any large clumps of mucus in the samples to mitigate errors in the rheological data due to inhomogeneity.

In most vertebrates, including fish, the predominant mucus-forming macromolecules are glycoproteins (mucins) that tend to swell in water by entanglements or chemical cross-linking and create a gel-like material[12-13,17-20]. The high-molecular-weight gel-forming macromolecules and high-water content reflects the slipperiness in the mucus[13]. A high degree of inter-macromolecular interactions leads to gel-formation whereas lower levels of inter-macromolecular interactions or broken bonds result in high-viscosity fluids[21].

The processes of food particulate filtration in filter feeding fish are aided by GR mucus-related properties such as cohesion and viscosity that determine its potential for adhesion and tack[22]. The strength of mucus-based adhesion depends on specific intermolecular interactions, electrostatic or hydrophobic interactions[23]. Sanderson et al.[24] conducted a suspension-feeding study in blackfish wherein they found the evidence for mucus-based adhesion. They stated that the adhesion of suspended food particulates with a mucosal surface is followed by the transport of aggregated clumps of particles bound together with mucus by directed water-flow acting on it[24]. Endoscopic techniques were used to observe filtered particles[24]. The mucus exposed to shear strain rates generated from water-flow facilitates the delivery of food particulates to digestive organs.

Literature on the range of shear rates and practical limits in the rheological testing of GR mucus is scarce. Therefore, guidance was sought from rheological studies on gastric, nasal, cervical and lung mucus, salmon skin mucus, hagfish slime, and bone-joint surface lubricant wherein the rheological characterization and non-Newtonian attributes of the mucus has been ascertained previously[11-12,25-31]. More recently, the effect of fish skin mucus on locomotion and propulsive efficiency has been studied using constant shear rate viscometry. Skin mucus rheology studies (without any dilution or homogenization) pertaining to seabream, sea bass and meagre demonstrated non-Newtonian behavior at typically low shear rates[14]. In another related study, the raw skin mucus samples from dorsal and ventral sides of the Senegalese sole were found to exhibit non-Newtonian behavior, indicating a higher viscosity of the ventral mucus at all shear rates considered[32]. Other rheological protocols pertaining to the hydrogel scaffold development and for highly concentrated suspensions using a constant shear rate viscometer have also been reported in the literature[33-34].

The GR mucus properties investigated using a strain rate controlled, rotational rheometer describe the rheology of complex biological fluids[25]. For Newtonian fluids, the apparent viscosity remains constant, is shear-rate-independent and the shear stresses vary linearly with shear strain rates (**Figures 3A,B**). For non-Newtonian fluids (such as shear-thinning fluids) viscosity is shear-rate-dependent or deformation-history-dependent (**Figure 3A,B**). The loss modulus (G") represents the extent to which the material resists the tendency to flow and is representative of fluid viscosity (**Figure 4**). The storage modulus (G') represents the tendency of the material to recover its original shape following stress-induced deformation and is equivalent to elasticity (**Figure 4**). The phase angle (δ) or loss tangent value, is calculated from the inverse tangent of G"/G'. It represents the balance between energy loss and storage and is also a common parameter for characterizing viscoelastic materials (δ = 0° for a Hookean solid; δ = 90° for a viscous liquid; δ < 45° for a viscoelastic solid and δ > 45° for a viscoelastic liquid) (**Figure 4**)[25]. The apparent yield stress (σ_y) in structured fluids represents a change of state that can be observed in rheological data from steady state sweep and dynamic stress-strain sweeps[10]. If the external applied stress is less than the apparent yield stress, the material will deform elastically. When the stress exceeds the apparent yield stress (marked as "average stress" in **Figure 3B**), the material will transition from elastic to plastic deformation and begin to flow in its liquid state[35]. Measuring the storage modulus (G') and loss modulus (G") in the mucus-sample under oscillatory stress (or

strain) conditions quantifies the change in the material state from gel-like to viscoelastic liquid-like behavior.

The types of rheometer tests performed to monitor data pertaining to storage modulus (G'), loss modulus (G") and apparent viscosity (η) are described here. The dynamic oscillation tests (strain sweeps and frequency sweeps) monitored G' and G" under controlled oscillation of cone geometry. The dynamic strain sweep tests determined the linear viscoelastic region (LVR) of the mucus by monitoring the intrinsic material response (**Figure 4**). Strain sweeps were used to determine the yielding behavior at constant oscillation frequency and temperature. The dynamic frequency sweep tests monitored the material response to increasing frequency (rate of deformation) at a constant amplitude (strain or stress) and temperature. Strain was maintained in the linear viscoelastic region (LVR) for the dynamic frequency sweep tests. The steady-state shear rate tests monitored the apparent viscosity (η) under steady rotation of the cone geometry. The GR mucus was subjected to incremental stress steps and apparent viscosity (η, Pa.s) was monitored for varying shear rate ($\dot{\gamma}$, 1/s).

The protocol presented in this paper treats the GR mucus as a complex structured material of unknown viscoelasticity with a certain linear viscoelastic response range. The fish mucus was extracted from the GRs of the silver carp during a fishing expedition at the Hart creek location in the Missouri River[1-2,36]. An array of GRs inside the mouth of a Silver carp is shown in **Figure 5A** and a schematic drawing is presented in **Figure 5B**. An excised GR is shown in **Figure 5C.** Extraction of mucus from GRs of the silver carp is summarized in the schematic drawings, **Figures 5D,E**. All the rheometer tests were performed under a constant, controlled temperature of 22 ± 0.002 °C, the temperature recorded at the fishing site[1-2,36]. Each mucus sample was tested three times with the rheometer, and the averaged results are presented in figures along with the statistical uncertainty bars.

PROTOCOL

1. Preparation of the mucus solutions of various concentrations

NOTE: Three concentrations of the mucus solution (400 mg/mL, 200 mg/mL and 100 mg/mL with approximate volumes, 1 mL, 1 mL, and 2 mL, respectively) are prepared for this experiment.

1.1 To calculate the mass of the mucus, measure the average mass of the vials ($M_{with-mucus}$; mg) with and without mucus (M_{vials} ; mg). Then subtract the mass of the vials with mucus with that without mucus ($M_{mucus} = M_{with-mucus} - M_{vials}$; mg).

1.2 Dilute the mucus into three concentrations (400, 200, 100, mg/mL) with deionized (DI) water.

1.2.1 Prepare the first concentration of the mucus solution, 400 mg/mL by adding 0.6 mL DI water to the mucus using a micropipette.

NOTE: Since the approximate volume of the extracted mucus was 1.4 mL, the 400 mg/mL solution will have a total volume of ~ 2 mL.

1.2.2 Place the 400 mg/mL mucus solution vial on a shaker to make sure that the mucus solution is adequately homogenized, and any mucus particulate agglomeration is mitigated.

1.2.3 Prepare the second concentration of the mucus solution, 200 mg/mL, by drawing half the volume of the first-concentration mucus solution into a new vial using a micropipette and adding 1 mL of DI water into the new vial.

1.2.4 Repeat step 1.2.2 for the first and second vials with mucus solutions.

1.2.5 Prepare the third concentration of the mucus solution, 100 mg/mL, by drawing half the volume (1 mL) of the 200 mg/mL solution into a new vial using a micropipette and add 1 mL of DI water into the new vial.

1.2.6 Repeat step 1.2.2 for all three concentrations of mucus solutions in their respective vials (see **Supplementary Figure 1**).

1.2.7 Store the mucus solution vials in a refrigerator until the rheometer calibration and testing is performed.

2 Measurements and data acquisition using a rheometer

NOTE: The software used in this protocol for instrument control and data acquisition with rheometer are noted in the **Table of Materials.** This software will be referred as 'rheometer instrument control software'.

2.1 Set up and calibrate the rheometer instrument.

2.1.1 Turn on the compressed air supply to the rheometer and make sure the pneumatic table and the rheometer are leveled using a bubble gauge. Twist off the protective cap on the rheometer shaft and hold shaft still whilst unscrewing.

2.1.2 Turn on the rheometer main switches to activate the magnetic bearings on the rheometer.

2.1.3 Turn on the rheometer control computer with the rheometer instrument control software installed in it and launch the rheometer instrument control software (see **Supplementary Figure 2**).

2.1.4 Perform instrument calibration by selecting the tabs, '**Calibration | Instrument**' from the software window. Choose '**Instrument**' option. Click on '**Calibrate**' under '**Inertia**'. Record the

instrument inertia calibration value in $\mu N.m.s^2$ and repeat calibration at least 3x to ensure calibration values are within 10% of each other (see **Supplementary Figure 3**).

2.2 Install the rheometer geometry on the shaft of the rheometer.

2.2.1 Click the '**Geometries**' tab in the rheometer instrument control software.

2.2.2 Clean the cone with the desired geometry, the 40 mm diameter, 1° 0' 11'' cone, and Peltier plate with isopropanol (see **Table 1, Table of Materials**, **Figure 1,** and **Figure 2**).

NOTE: The Peltier Plate comes installed on the rheometer; it can be cleaned with isopropanol while it is directly fixed to the rheometer.

2.2.3 Ensure that the Peltier plate fixture is free from any visible dust and clean, if necessary, with isopropanol. Install the Peltier plate if it is not pre-installed in the rheometer and connect the heat sink connections.

2.2.4 Press the '**Lock button**' on rheometer to the lock shaft that is connected to the cone geometry. This arrests the position of the shaft, but it can rotate freely at the position.

2.2.5 Click on '**Smart Swap | Enabled**' in the rheometer instrument control software tab to allow automatic detection of the geometry (see **Supplementary Figure 4**).

2.2.6 Turn the shaft on top of the rheometer to screw on geometry. The software will detect the 40 mm diameter, 1° 0' 11'' cone angle geometry at this stage (see **Table 1** and **Table of Materials**).

2.2.7 Repeat steps 2.2.5 – 2.2.6 to ensure that the geometry is detected.

2.2.9 Select '**Gap**' under the '**Control Panel**' of the rheometer instrument control software, click on '**Options**' icon and chose '**Axial Force**' option. Set axial force to '**1 Newton**'; this is to ensure the cone geometry touches the Peltier plate for zero gap initiation (see **Supplementary Figure 5**).

2.3 Perform the rheometer geometry calibration.

2.3.1 Select the tab, '**Geometry**' from the software window. Click on '**Calibrate**' under '**Inertia**'. Record the geometry inertia calibration value in $\mu N.m.s^2$ and repeat this 2-3 times to ensure calibration values are within 10% of each other.

2.3.2 Click on '**Calibrate**' under '**Friction**' in the software window. Record the geometry friction calibration value in $\mu N.m/(rad/s)$ and repeat this 2-3 times to ensure calibration values are within 10% of each other (see **Supplementary Figure 6**).

2.4 Perform the zero-gap initialization

NOTE: Since the geometry cannot be accurately raised above the Peltier Plate to perform measurements without a reference “zero” position, zero-gap initialization is performed. For the measurement purposes, the geometry has a built-in geometry gap of 24 µm and a trim gap of 28 µm. The trim gap is set to effectively clean the excess fluid that may spill outside the surface area of the geometry. These gaps are imperative for accurately measuring data using the sample and the rheometer. The step 2.4.1 is absolutely required to make sure that the geometry is set to zero gap for achieving the geometry and trim gaps of 24 µm and 28 µm, respectively.

2.4.1 Click on the ‘**Zero gap**’ icon under ‘**Gap**’ tab in the ‘**Control Panel**’ in the software window. The initialization is complete when the axial force experienced by the geometry is greater than or equal 1 N, as it touches the Peltier plate. Ensure that the rheometer gap is zeroed so that its reference position is accurate (see **Supplementary Figure 7** and **Supplementary Figure 8**).

2.4.2 Press ‘**up and down arrow**’ controls on the rheometer instrument or ‘**geometry raise and lower**’ icons under the ‘**Gap**’ tab in the rheometer instrument control software to raise the geometry to any arbitrary height. The control screen on the rheometer instrument and the control panel of the rheometer instrument control software will display the (same) gap height.

2.5 Set up the experimental procedure in the rheometer instrument control software. Perform the characterization of rheological properties by using a cone-on-Peltier plate geometry at 22 °C.

NOTE: The US Geological Survey website was used to ascertain the river water temperature River on September 20, 2018, when the silver carp used for the GR mucus experiments were fished at the Hart Creek location[36]. The temperature of the mucus can affect the rheological properties. The significance of adjusting the values to river temperature is to approximately match the temperature under which the mucus properties can be realistically estimated.

2.5.1 Select the tab, '**Experiments**' in the rheometer instrument control software and fill in the relevant information such as '**Name**', '**Operator**', '**Project**' etc. (see **Supplementary Figure 9**)

2.5.2 Select the tab, '**Geometry**' and make sure the information agrees with steps 2.2.5. - 2.2.7. (see **Supplementary Figure 10**).

2.5.3 Select the tab, '**Procedure**', and use the arrow keys set up '**1: Oscillation Amplitude**' procedure. (see **Supplementary Figure 11**).

2.5.4 Initialize '**Environmental Control**' settings as the following: 'Temperature = 22 °C'; 'Soak Time = 120 s' and check the box 'Wait for Temperature'.

2.5.5 Initialize '**Test Parameters**' settings as the following: 'Frequency = 1 Hz'; set 'Logarithmic sweep'; 'Torque = 10 to 10000 µN.m'; 'Points per decade = 5'.

2.6 Determine the Linear Viscoelastic Range (LVR) of the mucus of known concentration (100 mg/mL)

2.6.1 Using an appropriate micropipette and pipette tip draw approximately 0.3 mL of fish mucus solution of concentration 100 mg/mL (see Step 1.2, **Table of Materials**).

2.6.2 Introduce the mucus solution on to the Peltier plate using the micropipette (see **Figure 2**).

2.6.3 Press '**Trim Gap**' button on rheometer to lower the geometry on to the Peltier plate. Alternatively, click on '**Trim Gap**' icon under '**Gap**' tab in the '**Control Panel**' option in the rheometer instrument control software (see **Supplementary Figure 12**).

2.6.4 Use the micropipette with the pipette tip to remove any excess mucus solution and ensure that the fluid is underneath the geometry without any spilling near the periphery of the geometry.

NOTE: Improper loading of the fluid will lead to errors in the measurements. Under filled sample will lower torque distribution and over filled sample will lead erroneous stress distributions due to spilling along the edges.

2.6.5 Select '**Motor**' and '**Velocity**' tabs to 5 rad/s and 0 rad/s alternately, until there is minimal inertia and velocity in the sample underneath the geometry. The control screen on the rheometer instrument and the control panel of the rheometer instrument control software will display the gap inertia and velocity (see **Supplementary Figure 13**).

2.6.6 Press '**Geometry Gap**' button on rheometer to lower geometry to the preset suitable gap per specific geometry. Alternatively, click on '**Geometry Gap**' icon under '**Gap**' tab in the '**Control Panel**' option in the rheometer instrument control software (see **Supplementary Figure 14**).

2.7 Run the experiment to determine the Linear Viscoelastic Range (LVR) of the mucus of the known concentration (100 mg/mL).

2.7.1 Click '**Start**' icon on the rheometer instrument control software (see **Supplementary Figure 15**).

NOTE: The rheometer performs automatic measurements; once the '**Start**' button is pressed, the rheometer will take approximately 20 min to complete the test. The 'Points per decade' setting in Step 2.5.5 determines how much time the rheometer will need to complete measurements.

2.7.2 Run the experiment by clicking '**Yes**' on the pop-up box that appears and suggests that the geometry gap be lowered to the correct distance to start the experiment, if not already lowered.

2.7.3 Observe the real time plot generated by the rheometer that reports the loss (G') and storage (G'') moduli.

NOTE: The G' and G" are the storage and loss moduli, respectively. The storage modulus represents the tendency for the material to recover its original shape following stress-induced deformation and is equivalent to elasticity. The loss modulus represents the extent to which the material resists the tendency to flow and is representative of fluid viscosity (see **Figure 4**).

2.7.4 Set the X-axis of the plot to '**Oscillation strain percentage**'. To do this, right click on the graph presented and choose the '**Graph Variables' tab** (see **Supplementary Figure 16**).

2.7.5 Record the oscillation strain percentage range from the plot before material enters the Non-Linear Viscoelastic range, once the test is complete.

2.7.6 Press '**up and down arrow**' controls on the rheometer instrument or '**geometry raise and lower**' icons under the '**Gap**' tab in the rheometer instrument control software to raise the geometry to any arbitrary height above the Peltier plate.

2.7.7 Save the file that contains both the experimental procedure and results in the native file format of the rheometer instrument control software to ascertain the linear viscoelastic region (LVR) of the mucus sample.

NOTE: This can be done with the strain amplitude (%) and oscillation stress ($\bar{\sigma}$) before the data enters the non-linear viscoelastic region (NLVR).

2.8 Run the dynamic sweeps and steady state shear rate flow test experiments in Linear Viscoelastic Range (LVR) for the mucus of known concentration 100, mg/mL to generate results from three independent mucus samples of 100 mg/mL. Perform these steps on the available mucus concentration samples individually.

2.8.1 Repeat steps 2.5.1 – 2.5.4.

2.8.2 Initialize '**Test Parameters**' settings as the following: 'Frequency = 1 Hz'; set 'Logarithmic sweep'; 'Strain % = 100 to 10000 %; 'Points per decade = 10'.

2.8.3 Select the '**Procedure**' tab and use the arrow keys set up '2: Oscillation Frequency' procedure.

2.8.4 Initialize '**Environmental Control**' settings as the following: 'Temperature = 22 °C'; 'Soak Time = 0.0 s'.

2.8.5 Initialize '**Test Parameters**' settings as the following: 'Strain % = 1 %'; set 'Logarithmic sweep'; 'Frequency = 20 to 1 Hz'; 'Points per decade = 10'.

2.8.6 Select the '**Procedure**' tab and use the arrow keys set up '3: Flow Sweep' procedure.

2.8.7 Initialize '**Environmental Control**' settings as the following: 'Temperature = 22 °C'; 'Soak Time = 0.0 s'.

2.8.8 Initialize '**Test Parameters**' settings as the following: 'Shear rate = 1 to 10000 1/s'; set 'Logarithmic sweep'; 'Frequency = 20 to 1 Hz'; 'Points per decade = 10'; check box 'Steady state sensing'.

2.8.9 Repeat steps 2.7.1 – 2.7.2 and wait until the experiment is complete, approximately 45 minutes.

2.8.10 Press '**up and down arrow**' controls on the rheometer instrument or 'geometry raise and lower' icons under 'Gap' tab in the rheometer instrument control software to raise the geometry to any arbitrary height.

2.8.11 Use disposable wipes and gloves to remove and clean the mucus on the Peltier plate with isopropanol solution (see **Table of Materials**).

2.8.12 Save the file that contains both the experimental procedure and results in the native file format of the rheometer instrument control software.

3 Repeat the protocol for other concentrations of mucus solutions of 200 mg/mL and 400 mg/mL.

3.1 Perform steps 2.5 – 2.8 including all the sub-steps listed therein for the remaining two concentrations of mucus solutions, 200 mg/mL and 400 mg/mL.

4 Graphical representation and data analysis

NOTE: The code provided in the supplemental code file performs data averaging and generates repeatability-errors, overlays the data from all experiments. The standard-deviation calculation features are not available in the rheometer instrument control software. The code is written in a programming language for data analysis, post-processing and graphical representation (see **Table of Materials** for details).

4.1 Export data generated from step 2.8 pertaining to the 100 mg/mL GR mucus concentration and step 3.1 pertaining to the 200mg/mL and 400 mg/mL GR mucus concentrations into spreadsheet-format by clicking on the tab, '**File | Export | Excel**' in the rheometer instrument control software (see **Supplementary Figure 17**).

4.2 Run supplemental codes to generate plots of apparent viscosity (η) for varying shear strain rates ($\dot{\gamma}$) and loss modulus (G"), storage modulus (G') and phase angle (δ) for varying oscillation stress ($\bar{\sigma}$) and generate representative results.

REPRESENTATIVE RESULTS

In this section, we present the results of the experiments on GR mucus using a rotational rheometer with a cone geometry (40 mm diameter, 1˚ 0’ 11’’) and a Peltier plate. The experiments helped in characterizing the non-Newtonian, shear-thinning behavior of the GR mucus and the apparent yield stress depicting the mucus transition from a gel-like material to a fluid-like material. The representative results entail quantitative descriptions of low-torque limits and secondary flow effects of the rotational rheometer instrumentation. The instrumentation limits and steady-state and dynamic strain rate measurements helped in accurately ascertaining the viscoelastic behavioral trends and apparent yield stress of GR mucus. The apparent yield stress measurements provided a means to observe the minimum stress required for irreversible plastic deformation of the GR mucus and to initiate the flow. The flow initiation tendency of the GR mucus could be attributed to the food particulate adhesion and transport functions. The adhesion and transport functions of GR mucus were macroscopic material attributes that were informed by the rheological measurements in the protocol experiments. Therefore, macro-rheology characterization of the GR mucus was performed with this protocol.

The mucus used in the experiment was acquired from several gill rakers of up to three silver carp and did not have any visible traces of blood[1-2]. The acquired sample was diluted into two additional samples, as described in the protocol. All measurements were made at the controlled temperature of 22 ± 0.002 °C[36]. This temperature was maintained on the Peltier plate of the rheometer. The cone geometry was chosen for its versatility in measuring a wide range of viscosities in biological materials such as the GR mucus. The minimum torque under steady state shear conditions (10 x 10^{-9} *Nm*), minimum torque under oscillatory conditions (2 x 10^{-9} Nm) along with the cone angle (1° 0’ 11”) and the summary of rheometer specifications required for assessing low-torque and secondary flow regimes are presented in **Table 1**. We report replicates of final three samples for the characterization and comparison of non-Newtonian and shear thinning behavior.

Broad inferences after successful execution of the protocol

The successful execution of the protocol and analysis resulted in the characterization of (macro) rheological properties entailing non-Newtonian, shear thinning behavior of mucus extracted from the gill rakers of the silver carp, *Hypophthalmichthys molitrix.* Particularly, the yielding phenomenon was resolved and an apparent yield stress of the mucus (400 mg/mL concentration, closest to the actual extracted mucus consistency) was ascertained ($\sigma_y = 0.2736\ Pa$). The protocol was well-suited for measurements involving very small sample volume (approximately, 1.4 mL) of mucus. Due to scarcity of literature pertaining to GR mucus characterization, these data will aid in analytical modeling and extended rheometric studies.

Results of dynamic sweep experiments

The results of the dynamic frequency and amplitude sweep experiments are presented in this section. These are the results of the procedures created in steps 2.8.2 - 2.8.5. Low-torque limit for oscillatory frequency sweep and amplitude sweep of the GR mucus with 400 mg/mL concentration is marked in **Figures 6A,B**.

The frequency sweep data (**Figure 6A**) were acquired within an angular frequency range, $6.28 \leq \omega \leq 125.66\ rad\ s^{-1}$ at a constant oscillatory strain amplitude of 0.01. The choice of the strain amplitude value was derived from the linear viscoelastic region ascertained in protocol step 2.7. Most of these data fell within the low-torque limit and were unsuitable for physical interpretation.

The amplitude sweep data (**Figure 6B**) were acquired at a fixed angular frequency (ω) of 6.28 rad/s (1 Hz). The angular frequency was chosen by estimating the possible mastication frequency involving the motion of palatal folds in the interstices of the gill rakers. It should be noted that the amplitude sweep data were not affected by the low-torque regime of the instrumentation (**Figure 6B**). Hence, these data were further analyzed for all three mucus concentrations (100 mg/mL, 200 mg/mL and 400 mg/mL) to determine the extent of viscoelasticity and yielding behavior.

The graphical representation shown in **Figure 4** was used as a guideline for extended analysis of the amplitude sweep experiments. The results of three mucus solutions with concentrations 100 mg/mL, 200 mg/mL and 400 mg/mL are discussed below.

The result for 100 mg/mL mucus concentration (**Figure 7A**), shows that at low oscillation stresses $(0.01 \leq \bar{\sigma} \leq 0.1\ Pa)$ the storage and loss moduli (G' and G") overlapped significantly. At oscillation stresses greater than 0.1 Pa, the storage modulus declines, indicating lower elasticity. The loss modulus, representative of viscosity, remains constant in the full range of oscillation stress $(0.01 \leq \bar{\sigma} \leq 0.5\ Pa)$. This phenomenon can be attributed to a Newtonian fluid-like behavior and is in agreement with the constant apparent viscosity of the 100 mg/mL mucus concentration (**Figure 7A, Figure 8A,B**). The corresponding phase angle (δ) data show that at moderate and high oscillation stresses $(0.05 \leq \bar{\sigma} \leq 0.3\ Pa)$, the values vary between 55˚ and 70˚ (**Figure 7D**). It can, therefore, be inferred that the 100 mg/mL mucus solution demonstrates fluid-like behavior, with negligible apparent yield stress.

As observed in **Figure 7B**, 200 mg/mL concentration at low oscillation stresses $(0.02 \leq \bar{\sigma} \leq 0.04\ Pa)$, the storage modulus (G') decreases but still remains greater than the loss modulus (G"). Within the oscillation stress range $(0.04 \leq \bar{\sigma} \leq 0.07\ Pa)$, there was a "crossover" region wherein the G' and G" values remain approximately equal. This region is marked in **Figure 7B** with dashed lines and corresponding oscillation stress values were noted $(0.04193 \leq \bar{\sigma} \leq 0.06467\ Pa)$. Beyond this region, G" attained a higher value than G' suggesting a transition to a fluid-like behavior. However, G" (representing viscosity) remained constant within the full range of oscillation stress $(0.01 \leq \bar{\sigma} \leq 0.5\ Pa)$. The phase angle data presented in **Figure 7E** show a higher degree of variance, especially in the oscillation stress range $(0.04193 \leq \bar{\sigma} \leq 0.06467\ Pa)$. From **Figures 7B,E** one can infer that there was transitional behavior of the fluid from linear viscoelastic to non-linear viscoelastic region. Further, the 200 mg/mL mucus concentration represented non-Newtonian characteristics and propensity to yield with in the oscillation stress range, $(0.04193 \leq \bar{\sigma} \leq 0.06467\ Pa)$. The non-Newtonian, shear-thinning

fluid-like behavior agreed with the apparent viscosity data presented in **Figure 8A** and corresponding stress variations in **Figure 8B**.

The 400 mg/mL mucus concentration data are presented in **Figure 7C**,**F**. The G' and G" trends in **Figure 7C** clearly demonstrate a yielding phenomenon with a crossover point between G" and G' occurring after sharp decline in G". The apparent yield stress (σ_y) value was recorded as 0.2736 Pa. Furthermore, G" > G' where oscillation stress ($\bar{\sigma}$) was less than the apparent yield stress ($\bar{\sigma} < \sigma_y$) and G" < G' where $\bar{\sigma} < \sigma_y$. This indicated a clear change in the state of the mucus from gel-like to a non-Newtonian fluid-like state. The phase angle data presented in **Figure 7F** shows a sharp increase at the apparent yield stress ($\sigma_y = 0.2736\ Pa$) from approximately 20˚ to 65˚. Such sharp increase in the phase angle can occur when the material undergoes yielding and starts to flow like a fluid. The non-Newtonian fluid-like behavior can be further supported with the results of steady state shear tests reported in **Figure 8A,8B**. The apparent yield stress as reported in steady state shear tests was 0.2272 Pa (**Figure 8A**).

Results of steady state shear rate experiments

The results of the steady state shear rate experiments are presented for three mucus solutions with concentrations 100 mg/mL, 200 mg/mL and 400 mg/mL in this section using graphical representations as a guideline (**Figures 3A**,**B**). These results correspond to the procedure initialized in protocol steps 2.8.6-2.8.8.

From the data presented in **Figure 8A**, at low-shear rates $(1 \leq \dot{\gamma} \leq 4\ s^{-1})$ the apparent viscosity data for 100 mg/mL concentration of mucus, falls within the low-torque regime and at high-shear rates $(2500 \leq \dot{\gamma} \leq 10000\ s^{-1})$ falls within a secondary flow regime. Considering these limits, the slope of data shown at low-shear rates was also absorbed with the low-torque regime for the 100 mg/mL mucus concentration. In **Figure 8B**, the corresponding stress variation with shear rate data indicated a small range of shear rates where the sample attained a 'stress-plateau'. This region can be neglected for yield stress estimation as the corresponding viscosity data are subject to low-torque effects. The 100 mg/mL mucus solution, therefore, behaves as a Newtonian fluid and remains independent of the shear rate with a constant apparent viscosity of $0.0033\ Pa\ s\ (\pm 0.0007\ Pa\ s)$.

As observed in **Figure 8A**, the 200 mg/mL concentration of mucus remained unaffected by low-torque limits and demonstrated a shear-thinning effect in the shear rate range, $1 \leq \dot{\gamma} \leq 15\ s^{-1}$. The zero-shear strain rate viscosity (η_o) was noted as $0.032\ Pa\ s\ (\pm 0.024\ Pa\ s)$ and the infinite-shear strain rate viscosity (η_∞) at shear rate $(\dot{\gamma}), 1995\ s^{-1}$, was noted as $0.00085\ Pa\ s\ (\pm 2.495\ x\ 10^{-5}\ Pa\ s)$. The shear thinning effect of the fluid was demonstrated with a slope of -1.8 within the shear rate range, $1 \leq \dot{\gamma} \leq 15\ s^{-1}$. The corresponding stress variation in **Figure 8B**, demonstrates a 'stress-plateau' that represents a yielding phenomenon with the average yield stress of $0.1446\ Pa\ (\pm 0.0037\ Pa)$.

The 400 mg/mL concentration of mucus is the least diluted and consequently, the closest in material consistency to the actual extracted GR mucus. In **Figure 8A**, note that the shear-thinning characteristic is well-defined for the 400 mg/mL mucus concentration when compared to the 200

mg/mL mucus concentration. The zero-shear (η_o) and infinite-shear strain rate viscosities (η_∞) at shear rate $(\dot{\gamma}), 2512\ s^{-1}$, were $0.137\ Pa\ s\ (\pm 0.032\ Pa\ s)$ and $0.00099\ Pa\ s\ (\pm 9.323\ x\ 10^{-5}\ Pa\ s)$, respectively. In addition, the slope of the shear thinning region was established as -0.91 within the shear rate range, $1 \leq \dot{\gamma} \leq 32\ s^{-1}$. The corresponding 'stress-plateau' from the stress variations with shear rate observed in **Figure 8B**, represents an apparent yield stress of $0.2272\ Pa\ (\pm 0.0948\ Pa)$.

FIGURE AND TABLE LEGENDS

Table 1: Specifications of Rheometer

Figure 1: CAD rendering of rheometer components. (**A**) 40 mm 1˚ cone geometry, (**B**) Peltier Plate attachment. The cone geometry is attached to the shaft of the rheometer, and the Peltier Plate is connected to the base of the instrument.

Figure 2: Placement of fluid onto the Peltier plate. The fluid should be placed in the center of the plate to ensure an even spread of fluid throughout the plate when the geometry is lowered.

Figure 3: Graphical representation of steady rheological properties. Variation of (**A**) Apparent Viscosity (η) and (**B**) Shear stress ($\dot{\gamma}$) with Shear Strain rate.

Figure 4: Graphical representation of dynamic rheological properties. Variation of Storage (G') and Loss (G") Modulii and Phase Angle (δ) with Oscillation Stress.

Figure 5: Schematics of a silver carp's gill raker (GR). (**A**) View of gill raker array and palatal folds inside the mouth of the carp (**B**) Schematic drawing of the gill raker array and Palatal folds (**C**) Excised gill raker (**D**) Schematic drawing of the gill raker with salient features (**E**) Location of the mucus extraction in the gill raker. Images 5A and 5C were taken during a dissection performed by Professor L. Patricia Hernandez of the Department of Biological Sciences at The George Washington University.

Figure 6: Low-torque effects. Storage and loss modulus variation for 400 mg/mL, mucus concentration with (**A**) Frequency sweeps at strain amplitude = 0.01 and (**B**) Amplitude strain = 1 Hz, ω = 6.28 rad/s.

Figure 7: Amplitude sweeps for three concentrations of Silver Carp mucus. Tests were completed at f = 1 Hz or ω = 6.28 rad/s (**A**) Storage and Loss modulus variation for mucus concentration, 100 mg/mL (**B**) Storage and Loss modulus variation for mucus concentration, 200 mg/mL (**C**) Storage and Loss modulus variation for GR mucus concentration, 400 mg/mL (**D**) Phase angle variation for GR mucus concentration, 100 mg/mL (**E**) Phase angle variation for mucus concentration, 200 mg/mL (**F**) Phase angle variation for mucus concentration, 400 mg/mL.

Figure 8: Variation of apparent viscosity (η) and stress (σ) with shear rate ($\dot{\gamma}$) for all three concentrations of fish mucus. (**A**) Apparent viscosity variation with shear rate for mucus

concentrations, 400 mg/mL, 200 mg/mL and 100 mg/mL along with regimes of low-torque effects and secondary flow effects marking the criterion for rejecting bad data (**B**) Stress variation with shear rate for GR mucus concentrations, 400 mg/mL, 200 mg/mL and 100 mg/mL, marking the 'stress plateaus' with dashed-lines. Dashed lines represent the average apparent yield stress values for the three GR mucus concentrations.

Supplementary Figure 1: Three concentrations of silver carp GR mucus. From left to right: 400 mg/mL DI water, 200 mg/mL DI water, 100 mg/mL DI water. The initial concentration of 400 mg/mL was chosen with the criteria that once diluted the sample would contain a reasonable amount of fish mucus while also providing a large enough volume to run several tests. The two subsequent concentrations were diluted by 50% of the volume.

Supplementary Figure 2: Launch of rheometer instrument control software. This software must be launched only after the machine is turned on. Otherwise, the instrument may not be calibrated correctly.

Supplementary Figure 3: Calibration of instrument. Inertial calibration is the only calibration needed for the instrument, but there are several other calibrations used for the geometry.

Supplementary Figure 4: Smart swap toggle. This was used for enabling or disabling smart swap. Smart swap is a rheometer instrument control software feature that automatically detects a geometry once it is placed on the rheometer shaft.

Supplementary Figure 5: Measurement Gap Options The **"**gap" tab options were accessed to set the conditions for zero gap mode and traverse velocity of the measurement head. An axial contact force between the geometry and the Peltier plate was set to 1 N to ensure the zero-gap reference, i.e., the contact between cone geometry and the surface of the Peltier plate. The measurement head was then made to accurately traverse to the measurement gap of 28 µm between the 40 mm 1˚ cone geometry and the Peltier plate.

Supplementary Figure 6: Calibration of geometry attachment. 40 mm 1˚ cone geometry is shown. The geometry was calibrated in the same way as the instrument calibration to ensure accurate measurements are taken during an experiment.

Supplementary Figure 7: Zero Gap icon. Once zero gap is complete, the rheometer can accurately reference the position of the shaft, with the geometry attached to it, as it is raised or lowered.

Supplementary Figure 8: CAD rendering of geometry and plate after zero gap completion.

Supplementary Figure 9: Step 2.5.1 of procedure. The figure represents the way sample naming and file and data output are set.

Supplementary Figure 10: Step 2.5.2 of procedure. The figure represents how geometry settings, such as sample volume, geometry gap, and trim gap can be set. For some geometries, namely the cone used in this experiment, these settings are unchangeable and defined based on the geometry.

Supplementary Figure 11: Step 2.5.3 of procedure. The figure represents how test setting and conditioning are set in this procedural step.

Supplementary Figure 12: Trim gap icon. The trim gap was set so that the geometry could be lowered enough to trim excess fluid that leaks out of area between the plate and shaft. The gap is dependent upon the geometry in use. For the geometry used in the protocol, the trim gap was 28 µm.

Supplementary Figure 13: Motor velocity icon. The motor settings were used to adjust speed of motor. The motor was turned on to aid in the removal of excess sample from the plate.

Supplementary Figure 14: Geometry gap icon. The geometry gap lowers geometry to a specific distance above the Peltier Plate as specified by the cone plate geometry. For the geometry used in the protocol, the geometry gap is 24 µm.

Supplementary Figure 15: Start icon. The start button initiates the entire sequence of procedures that were set up earlier.

Supplementary Figure 16: Changing the Graph Variables. The figure represents the variables that can be defined from running the procedure. Particularly, oscillation strain is of importance in the protocol.

Supplementary Figure 17: Exporting of rheometer instrument control software files to a spreadsheet software. After the files are exported as spreadsheets, the data analysis was made feasible using other programming software.

Supplemental Code File: Post-processing of data files using data analysis program.

DISCUSSION

One of the main objectives of developing this protocol is to establish that it is well-suited for rheological characterization of GR mucus when very small sample volumes are available. We acknowledge that more samples from a school of silver carp are needed to fully characterize the rheological properties of the GR mucus and the data presented herein are not a generalization across the entire silver carp population. Our technique is justified because its efficacy with rheological characterization of small sample volumes and can be used in extended investigations with larger mucus sample volumes.

The critical steps within the protocol are the preparation of mucus solutions of various concentrations, measurements and data acquisition using a rotational rheometer, and graphical representation and data analysis for physical insights.

Physical insights into GR mucus data are drawn from graphical representations shown in **Figure 3** and **Figure 4**, that are annotated with attributes of the expected material behavior. Zero-shear strain rate viscosity (η_o) values can be observed at low-shear strain rates where mobility of the material molecules dominates (**Figure 3A** and **Figure 8A**). Infinite-shear strain viscosity (η_∞) values in non-Newtonian fluids are orders of magnitudes lower than the zero-shear strain rate viscosity. These data can be noticed at high shear rates where there is little or no dependence on intermolecular interactions (**Figure 3A** and **Figure 8A**). For non-Newtonian fluids, apparent viscosities progressively decrease as the shear rates increase and attain a constant low value (**Figure 3A** and **Figure 8A**). Yielding behavior in the GR mucus under steady state measurements can be represented with slope as shown in **Figure 3A** and presented in Equation 1., where η_a represents the apparent viscosity, σ_y is the (constant) yield stress and $\dot{\gamma}$ is the shear strain rate.

$$\eta_a = \frac{\sigma_y}{\dot{\gamma}} \tag{1}$$

Figure 3A and **Figure 8B** are presented on a log-log scale and therefore, Equation 1 attains the following form:

$$log\ \eta_a = k - \log \dot{\gamma} \tag{2}$$

where k – represents the apparent yield stress. On a log-log scale, the apparent viscosity decreases with a slope of '-1' indicating material yield as shown in **Figure 3A**[10]. The 200 mg/mL and 400 mg/mL mucus concentrations possessed slopes of -1.8 and -0.91, respectively, and demonstrate the yielding behavior (**Figure 8A**). Under dynamic oscillation measurements, the viscoelastic characteristics are independent of the strain amplitude in the Linear Viscoelastic Region (LVR) (**Figure 4**). The yielding behavior in the GR mucus under dynamic oscillation measurements can be observed as the viscoelastic material (GR mucus) enters the non-linear viscoelastic region (NLVR) as the storage modulus (G') decreases (**Figure 4**). In the NLVR regime the viscoelastic material will demonstrate solid-gel-like behavior if the storage modulus is greater than the loss modulus (G' > G"). When the loss modulus exceeds the storage modulus (G' < G"), a "crossover" between G' and G" data occur. As shown in **Figure 7B,C**, the 200 mg/mL and 400 mg/mL GR mucus concentrations demonstrated fluid-like behavior marked by the "crossover" between G' and G" data. The apparent yield stress under steady state measurements is represented as the average value of stress until an inflection point is reached (**Figure 3B**). Thereafter, the stress begins to increase sharply with an increase in the shear strain rate as shown in **Figures 3B** and **Figure 8B**. The GR mucus data (200 mg/mL and 400 mg/mL concentrations) showed shear-thinning fluid behavior until the material begins to yield (**Figure 8A**,**B**). The apparent yield stress was observed clearly in 200 mg/mL and 400 mg/mL mucus concentrations due to their non-Newtonian characteristics (**Figures 8B**). The apparent yield stress under dynamic oscillation measurements are shown in **Figure 4** and **Figures 7A,C** as the "crossover" region between G' and G" data, followed by G" values exceeding G'. The 400 mg/mL GR mucus data

showed shear-thinning, non-Newtonian behavior. The onset point of material yield was observed with an apparent yield stress of approximately 0.2736 Pa (Figure 7C). The hydrogel-to-fluid like transition with phase angle ($\delta = \tan^{-1}(G''/G')$) changes are presented in Figures 4 and 7D-F. The extrema in the phase angle is associated with a Hookean solid at 0˚ and viscous fluid at 90˚ as shown in **Figure 4**. The phase angle values around 45˚ were attributed to transition of gel-like behavior of the material to a fluid-like behavior. The 400 mg/mL mucus concentration clearly showed a change in the material characteristic from hydrogel to fluid like behavior through the process of yielding with an apparent yield stress of ~ 0.2736 Pa (**Figure 7F**).

Understanding the measurement limitations and avoiding data unsuitable for physical interpretation is a challenge with complex and soft biological fluids, especially when working with small sample volumes[11]. The data generated under low-torque and secondary flow effects are unsuitable for physical interpretation and are dependent on the geometry used in the rheometer (such as cone and plate in this study). These regimes were identified to avoid any misrepresentation of experimental data suffering from instrument resolution and measurement artifacts due to momentum diffusion. Low-torque limits (**Figure 5B** and **Figure 8A**) are functions of geometry and minimum torque generated by the instrument (**Table 1**). Under steady shear measurement conditions, the criterion for rejecting data affected by the low-torque limit for a cone-plate geometry of radius (R) with minimum torque (T_{min} = 10 x 10^{-9} Nm, **Table 1**) has been discussed by Ewoldt et al. and is presented below[11]:

$$\eta > \frac{\left(\frac{3}{2\pi R^3}\right) T_{min}}{\dot{\gamma}} \tag{3}$$

where $\dot{\gamma}$ is the shear strain rate. The regimes of instrumentation limitation governed by low-torque and secondary flow effects are marked in **Figure 6A** and **Figure 8A**. Unlike the 100 mg/mL GR mucus concentrations, the 200 mg/ml and 400 mg/mL GR mucus concentrations were unaffected by low-torque effects clearly demonstrate non-Newtonian, shear thinning behavior with high zero-shear strain rate viscosities at low shear strain rates. The criterion for minimum measurable viscoelastic moduli under dynamic oscillation measurements has been discussed by Ewoldt et al. and presented below (Equation 4)[11]. In Equation 4, for a cone-plate geometry of radius (R) the minimum torque under oscillatory shear (T_{min} = 2 x 10^{-9} Nm, **Table 1**).

$$G_{min} = \frac{\left(\frac{3}{2\pi R^3}\right) T_{min}}{\gamma_0} \tag{4}$$

where G_{min} is the storage modulus (G') or loss modulus (G") and γ_0 is the shear strain rate. The regimes of instrumentation limitation governed by low-torque effects are marked in **Figures 6A,B**. The secondary flow regime under steady state measurements is governed by an inward momentum diffusion of the fluid by means of an eddy residing within the rotational cone and plate geometry[11]. The secondary flow pattern increases torque incorrectly making the fluid appear to be shear-thickening (**Figure 8A**). The secondary flow limit in **Figure 8A** was drawn using the following relation:

$$\eta > \frac{L^3/R}{Re_{crit}}\rho\dot{\gamma} \quad (5)$$

where L = βR, β is the cone angle, R is the cone radius, ρ = 1000 kg m^{-3}, Re_{crit} = 4 and $\dot{\gamma}$ is the shear rate. This regime helped in the accurately estimating the infinite-shear strain viscosity (η_∞) values in GR mucus samples.

A modification of the protocol can be made by using a flat-plate geometry instead of the cone-plate geometry as shown in protocol presented herein. The flat-plate tests should be performed with a parametric variation of the measurement gap in the rotational rheometer to reveal the dependence of apparent yield stress on the measurement gap and geometry. The suggested improvements of the protocol presented in this paper are described below. A parametric variation of the strain amplitude in the linear viscoelastic regime (LVR) and oscillation frequency should be performed. 'Tack and peel' rheology tests should be performed to develop a full understanding of the adhesivity of the GR mucus. Rheology characteristics of GR mucus should be performed on larger sample volume ensembles along with studies to measure any traces of blood cells to account of its effect on the overall GR rheological properties.

The limitations of the protocol are described below. The intricacies of the GR mucus extraction-procedures and the presence of blood cells or tissue fragments in the mucus samples may influence the rheology of the mucus. However, it should be noted the mucus used in the protocol did not have any visible traces of blood. The GR mucus sample is a heterogenous material and can possess different rheological properties due to the variance in location of and the conditions post-extraction. This limitation was addressed by sufficiently homogenizing the GR mucus using a shaker to breakdown any large clumps of mucus and tissue presence. Another important limitation is the very small GR mucus sample volumes (approximately 1.4 mL) that can be harvested for analyses that constrain a generalization of GR mucus properties.

The significance of this protocol is that it allows for an accurate rheological characterization of non-Newtonian, biological fluids such as the mucus. The protocol presented herein paves the way for investigating other similar biological fluids associated with human, animal and plant secretions. In addition, synthetic fluids or polymer-based solutions that are analogs of biological fluids can be testing using this protocol to understand material properties under varying stresses, oscillation frequencies, and temperature. The protocol is well-suited for rheological characterization of biological fluids when very small sample volumes are made available.

The extended outcome of the protocol is that the apparent viscosity and apparent yield stress of GR mucus will facilitate the creation of analytical models to interpret results from fundamental hydrodynamic investigation of filter feeding and advance technologies requiring and involving crossflow and membrane filtration.

The macro-rheological study is based on the hypothesis that the mucus in contact with food particulates is initially, in a gel-like state that serves as an adhesive. Upon initiation of flow and

shear forces the mucus attains an apparent yield stress and undergoes plastic deformation. The protocol execution using a rotational rheometer helped in characterization of the transition of mucus from gel-like to fluid-like behavior. This transition was experimentally observed, and the apparent yield stress was recorded at 0.2736 Pa in rotational rheometer experiments. When the external stresses on the mucus are less than the apparent yield stress, the mucus will demonstrate gel-like behavior to facilitate adhesion of food particulates. When the external stresses exceed the apparent yield stress, mucus will demonstrate shear-thinning behavior that will facilitate transport of agglomerated food particulates to the digestive organs in the silver carp.

ACKNOWLEDGMENTS:

The authors acknowledge support and funding from the GW Center for Biomimetics and Bioinspired Engineering. We thank Professor L. Patricia Hernandez of the Department of Biological Sciences at The George Washington University for inspiring the investigation and ongoing collaboration, providing biological expertise on the physiology of the silver carp and providing the mucus samples. We thank the students, Mr. David Palumbo, Ms. Carly Cohen, Mr. Isaac Finberg, Mr. Dominick Petrosino, Mr. Alexis Renderos, Ms. Priscilla Varghese, Mr. Carter Tegen and Mr. Raghav Pajjur for help in the laboratory and Mr. Thomas Evans and Mr. James Thomas of TA Instruments, New Castle, DE for support with training and maintenance of the rheometer. Images for Figure 5A,C were taken during a dissection performed by Professor L. Patricia Hernandez of the Department of Biological Sciences at The George Washington University.

DISCLOSURES:

No conflicts of interest declared.

REFERENCES:

1. Cohen, K. E., Hernandez, L. P. The complex trophic anatomy of silver carp, *Hypophthalmichthys molitrix*, highlighting a novel type of epibranchial organ. *Journal of Morphology*. **279**, 1615–1628 (2018).
2. Cohen, K. E., Hernandez, L. P. Making a master filterer: Ontogeny of specialized filtering plates in silver carp (*Hypophthalmichthys molitrix*). *Journal of Morphology.* **279**, 925–935 (2018).
3. Cremer, M., Smitherman, R. Food habits and growth of silver and bighead carp in cages and ponds. *Aquaculture*. **20** (1), 57–64 (1980).
4. Battonyai, I. et al. Relationship between gill raker morphology and feeding habits of hybrid bigheaded carps (*Hypophthalmichthys spp.*). *Knowledge and Management of Aquatic Ecosystems.* 416, 36 (2015).
5. Zhou, Q., Xie, P., Xu, J., Ke, Z., Guo, L. Growth and food availability of silver and bighead carps: Evidence from stable isotope and gut content analysis. *Aquaculture Research.* **40** (14), 1616–1625 (2009).
6. Freedman, J. A., Butler, S. E., Wahl, D. H. Impacts of invasive Asian carps on native food webs (Final Report). Urbana-Champaign, IL: University of Illinois, Kaskaskia Biological Station. (2012).

7. Nico, L., Fuller, P., Li, J. Silver carp (*Hypophthalmichthys molitrix*)—FactSheet. (2017).
8. Walleser, L., Howard, D., Sandheinrich, M., Gaikowski, M., Amberg, J. Confocal microscopy as a useful approach to describe gill rakers of Asian species of carp and native filter-feeding fishes of the upper Mississippi River system. *Journal of Fish Biology*. **85** (5), 1777– 1784 (2014).
9. Nelson, A. Z., Ewoldt, R. H. Design of yield-stress fluids: a rheology-to-structure inverse problem. *Soft Matter*. **13**, 7578—7594 (2017).
10. Chen, T. Rheological Techniques for Yield Stress Analysis. TA Instruments Applications Note, RH025 (2020).
11. Ewoldt, R. H., Johnston, M. T., Caretta, L. M. *Experimental challenges of shear rheology: how to avoid bad data.* in: S. Spagnolie (Editor), Complex Fluids in Biological Systems, Springer, (2015).
12. Thornton, D. J., Sheehan, J. K. From Mucins to Mucus: Toward a more coherent understanding of this essential barrier. *Proceedings of the American Thoracic Society*. **1**, 54 – 61 (2004).
13. Shepard, K. L. Functions for fish mucus. *Reviews in Fish Biology and Fisheries*. **4**, 401-429 (1994).
14. Fernández-Alacid, L., et al. Skin mucus metabolites in response to physiological challenges: A valuable non-invasive method to study teleost marine species. *Science of the Total Environment.* **644**, 1323-1335 (2018).
15. Wagner, C. E., Wheeler, K. M., Ribbeck, K. Mucins and Their Role in Shaping the Functions of Mucus Barriers. *Annual Reviews in Cell and Developmental Biology.* 34, 189–215, (2018).
16. Bird, R. B., Armstrong, R. C., Hassager O. *Dynamics of Polymeric Liquids, Volume 1: Fluid Mechanics*. New York: Wiley. 1,255–1284, (1987).
17. Mantle, M., Allen, A. Isolation and characterisation of the native glycoprotein from pig small intestinal mucus. *Biochemical Journal.* **195**, 267-275 (1981).
18. Allen, A., Hutton, D. A., Pearson, J. P., Sellers, L. A. *Mucus glycoprotein structure, gel formation and gastrointestinal mucus function.* In Nugent, J. and O'Connor, M., eds. *Mucus and Mucosa* (Ciba Foundation Symposium). London: Pitman, 137-156 (1984).
19. Asakawa, M. Histochemical studies of the mucus on the epidermis of eel, *Anguillajaponica. Bulletin of Japanese Society of Scientific Fisheries.* **36**, 83-87 (1970).
20. Fletcher, T. C., Jones, R., Reid, L. Identification of glycoproteins in goblet cells of epidermis and gill of plaice *(Pleuroneces platessa* L.), flounder *(Platichthys flesus* (L.)) and rainbow trout (Salmo *gairdneri* Richardson). *Histochemical Journal*. **8**, 597-608 (1976).
21. Silberberg, A. Mucus glycoprotein, its biophysical and gel forming properties. *Symposia of the Society for Experimental Biology.* **43**, 43-64 (1989).
22. Hills, B. *The Biology of Surfactants.* Cambridge: Cambridge Univ. Press. 408, (1988).
23. Aubert, H., Brook, A. J., Shephard, K. L. Measurement of the adhesion of a desmid to a substrate. *British Phycology Journal*. **24**, 293-295 (1989).
24. Sanderson, S. L., Cech, J. J., Patterson, M. R. Fluid dynamics in suspension feeding black fish. *Science.* **251**, 1346-1348, (1991).
25. Lai, S. K., Wang, Y. Y., Wirtz, D., Hanes, J. Micro- and macrorheology of mucus. *Advanced Drug Delivery Reviews*. **61**(2), 86-100 (2009).

26. Chaudhary, G., Ewoldt, R. H., Thiffeault, J. L. Unravelling hagfish slime. *Journal of Royal Society Interface.* **16** (150), 20180710 (2019).
27. Downing, S., Salo, W., Spitzer, R., Koch, E. The hagfish slime gland: a model system for studying the biology of mucus. *Science.* **214**, 1143–1145, (1981).
28. Hwang, S. H., Litt, M., Forsman, W. C. Rheological properties of mucus. *Rheologica Acta*, 8, 438-448, (1969).
29. Litt, M. Mucus rheology. *Archives of Internal Medicine.* **126**, 417 – 423, (1970).
30. Quarishi, M. S., Jones, N. S., Mason, J. The rheology of nasal mucus: a review. *Clinical Otolaryngology.* **23**, 403 – 413, (1998).
31. Nordgård, C. T., Draget, K. I, Seternes, T. Rheology of salmon skin mucus. *Annual Transactions - The Nordic Rheology Society.* 23, 175-179 (2015).
32. Fernández-Alacid, L., et al. Comparison between properties of dorsal and ventral skin mucus in Senegalese sole: Response to an acute stress. *Aquaculture*. 513, 734410 (2019).
33. Yüce, C., Willenbacher, N. Challenges in Rheological Characterization of Highly Concentrated Suspensions — A Case Study for Screen-printing Silver Pastes. *Journal of Visualized Experiments* (122), 55377 (2017).
34. Sultan, S., and Mathew, A. P. 3D Printed Porous Cellulose Nanocomposite Hydrogel Scaffolds. *J. Vis. Exp.* 146, (2019).
35. Barnes, H.A., Hutton, J. F., Walters, K. *An Introduction to Rheology*. Amsterdam: Elsevier, (1989).
36. "National Water Information System." *USGS Current Conditions for USGS 06910450 Missouri River at Jefferson City, MO*, U.S. Geological Survey, https://nwis.waterdata.usgs.gov/usa/nwis/uv/?cb_00010=on&cb_00060=on&cb_00065=on&format=gif_default&site_no=06910450&period=&begin_date=2018-09-19&end_date=2018-09-21.

Figure 1

Click here to access/download;Figure;Figure_1_wAB.tiff

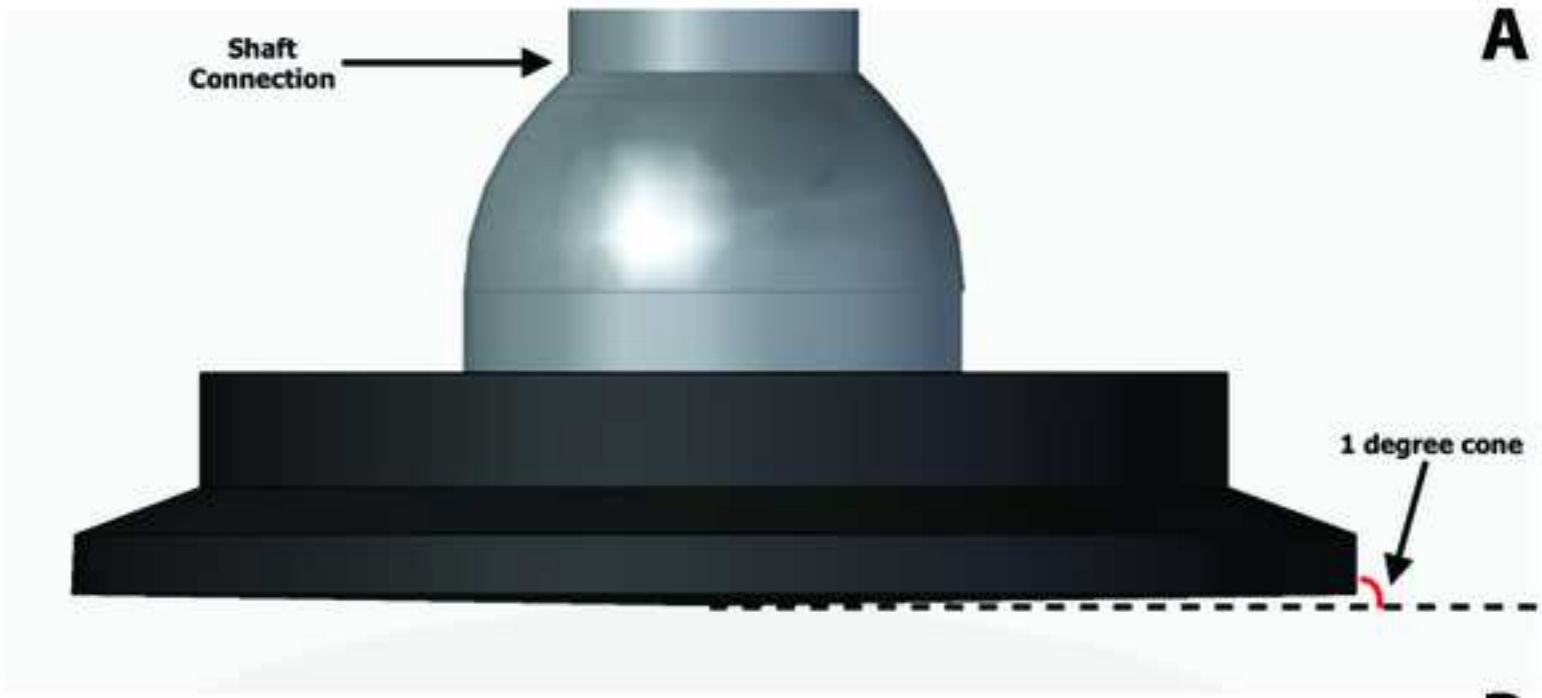

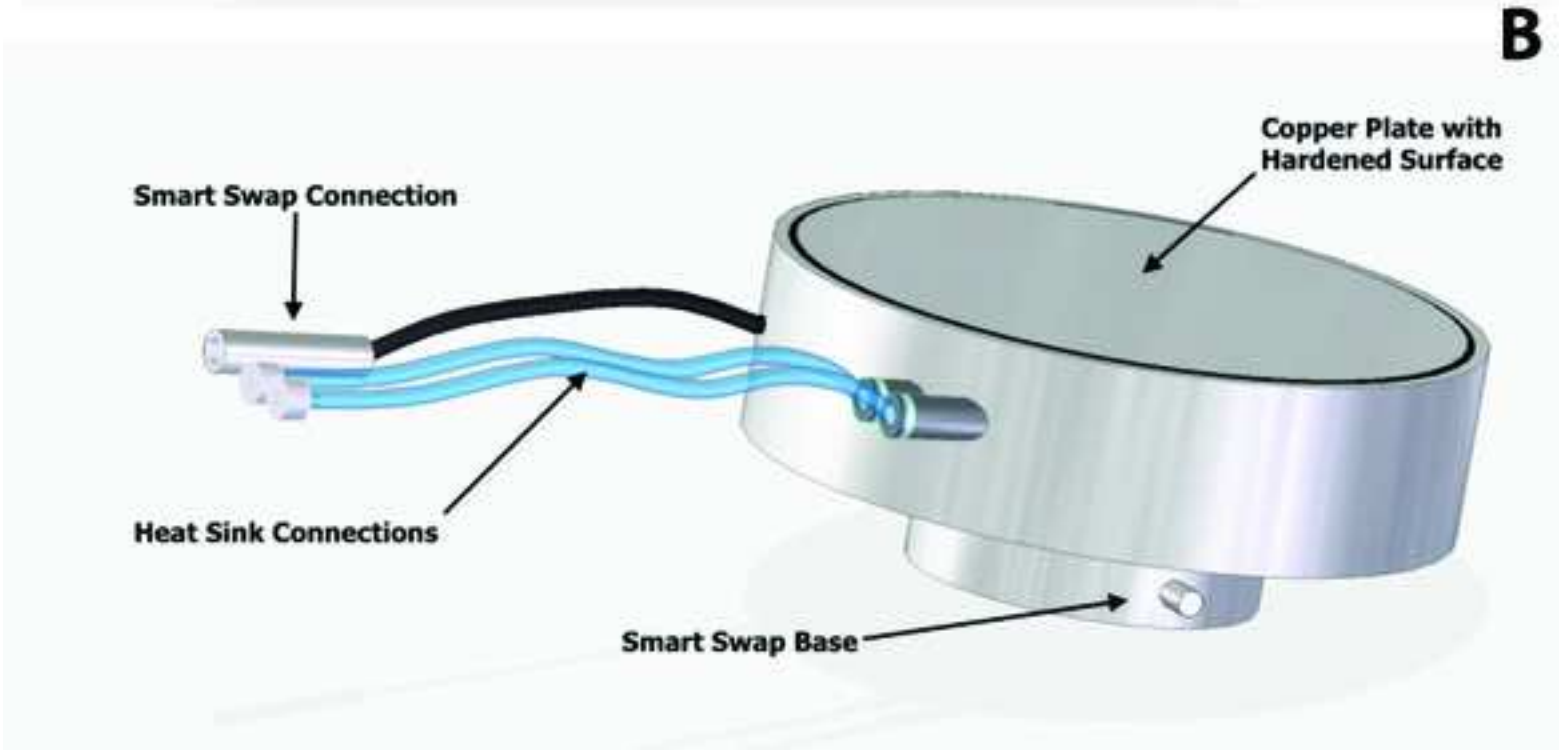

Figure2

Click here to access/download;Figure;Figure_2.tiff

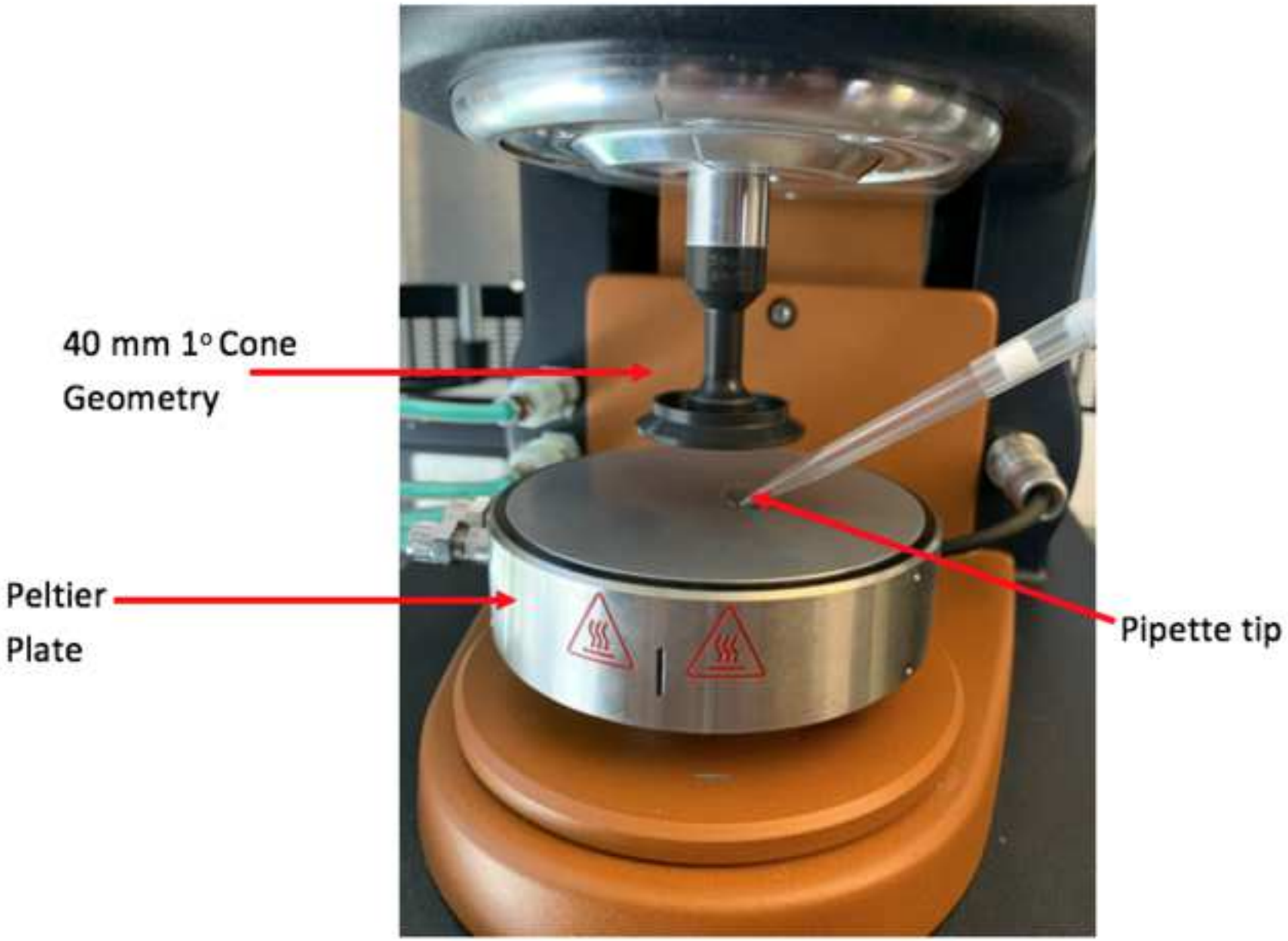

Click here to access/download;Figure;Figure_3.tif

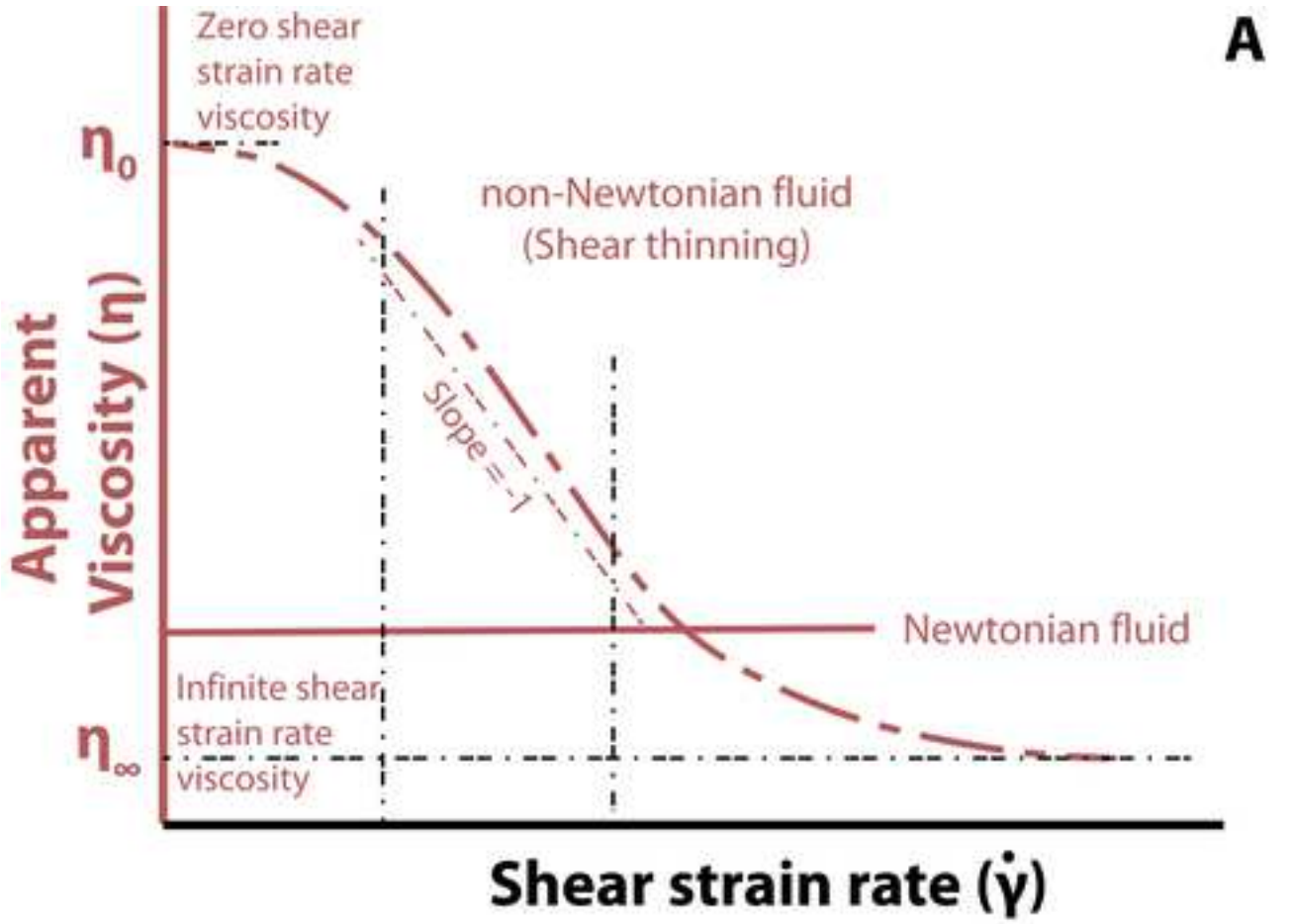

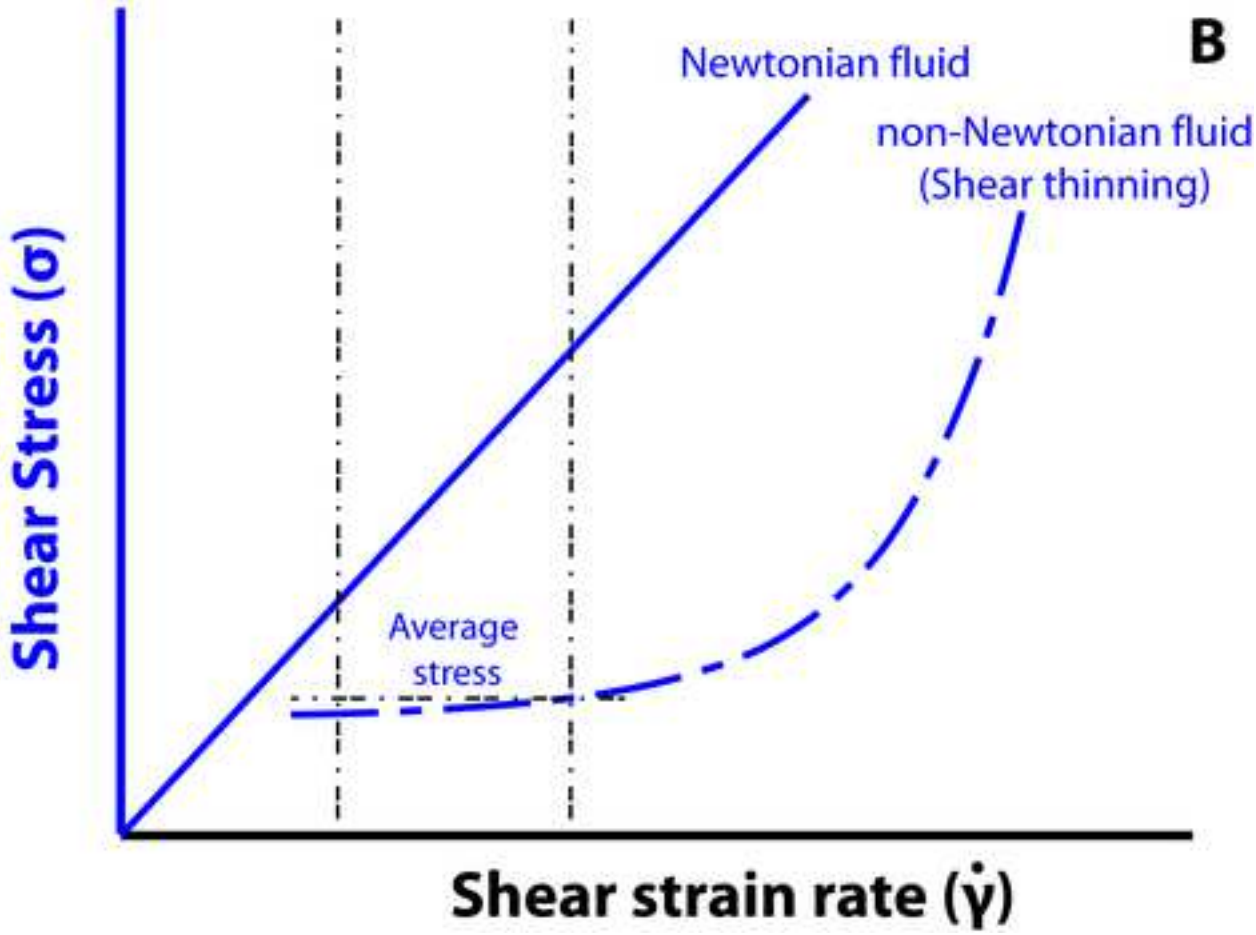

Click here to access/download;Figure;Figure_4.tif

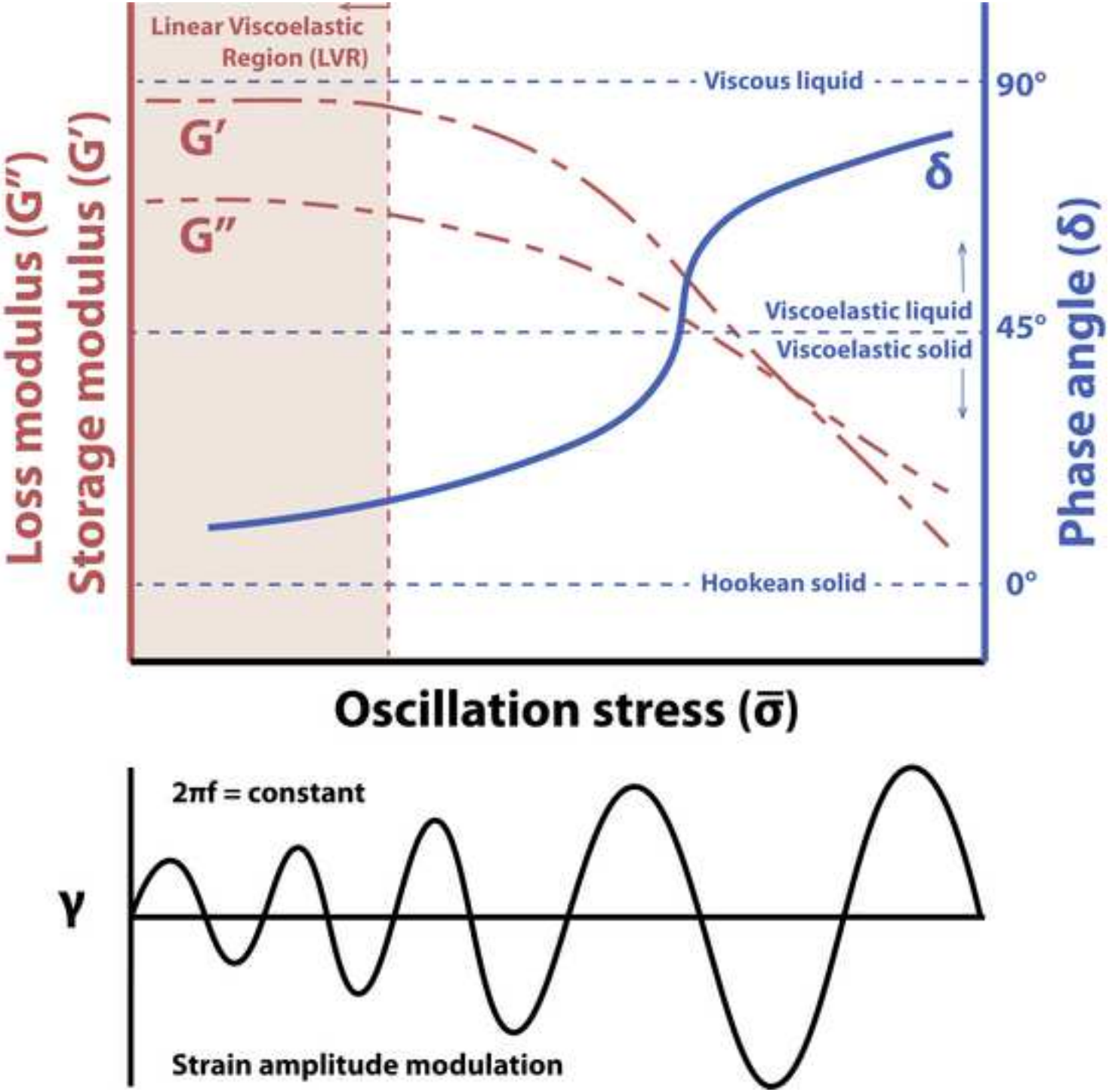

Click here to access/download;Figure;Figure_5.tif

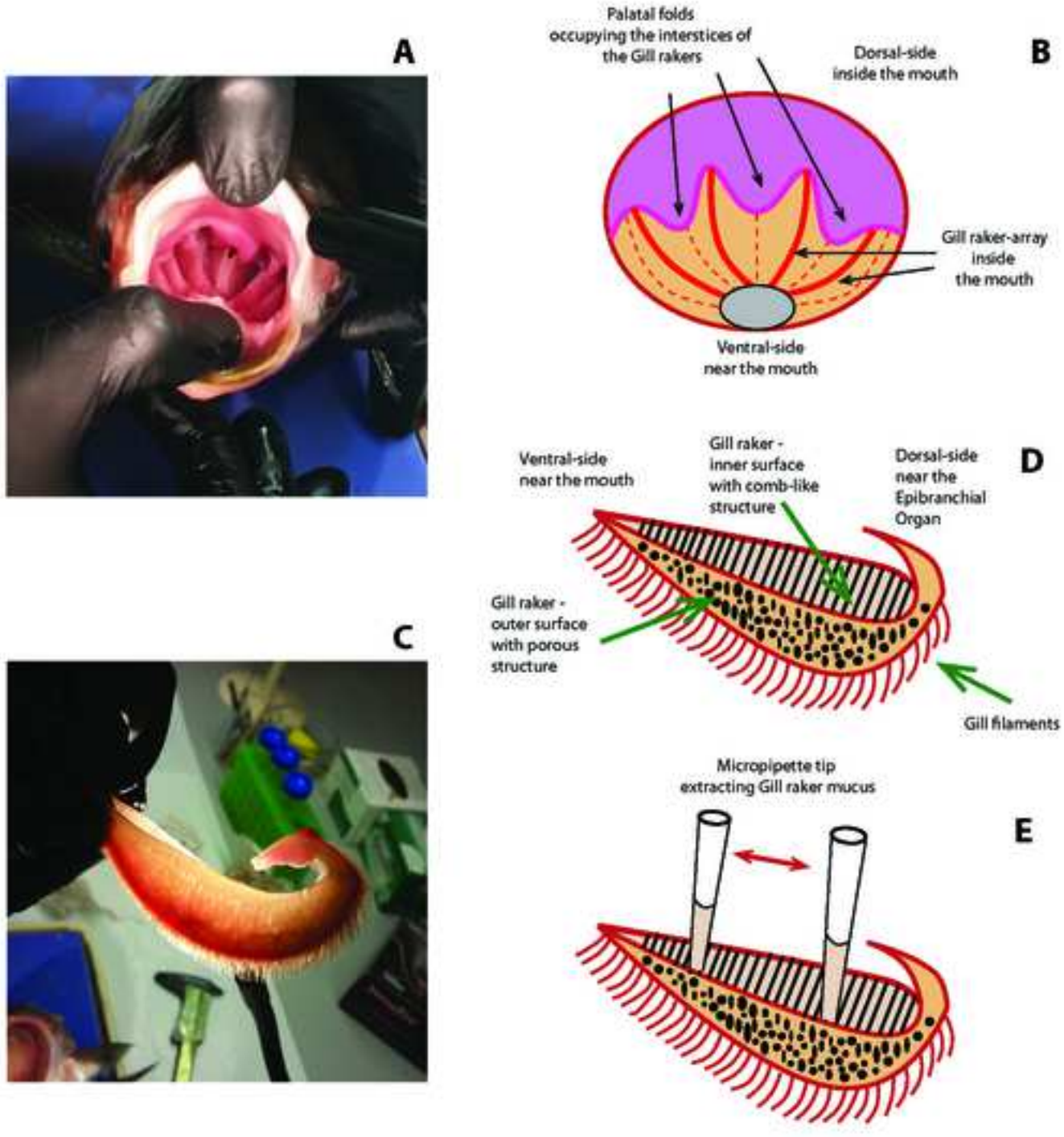

Figure6

Click here to access/download;Figure;Figure_6.tif

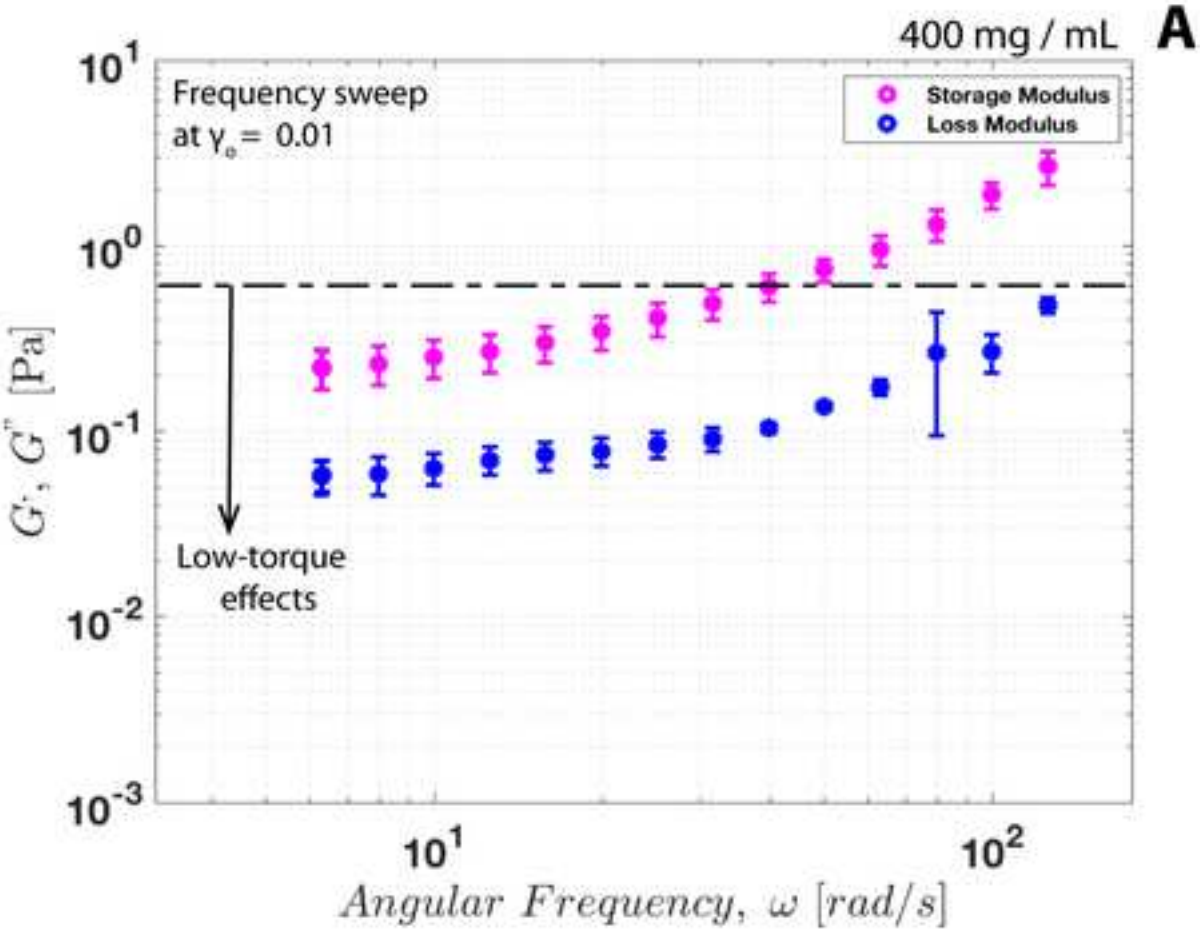

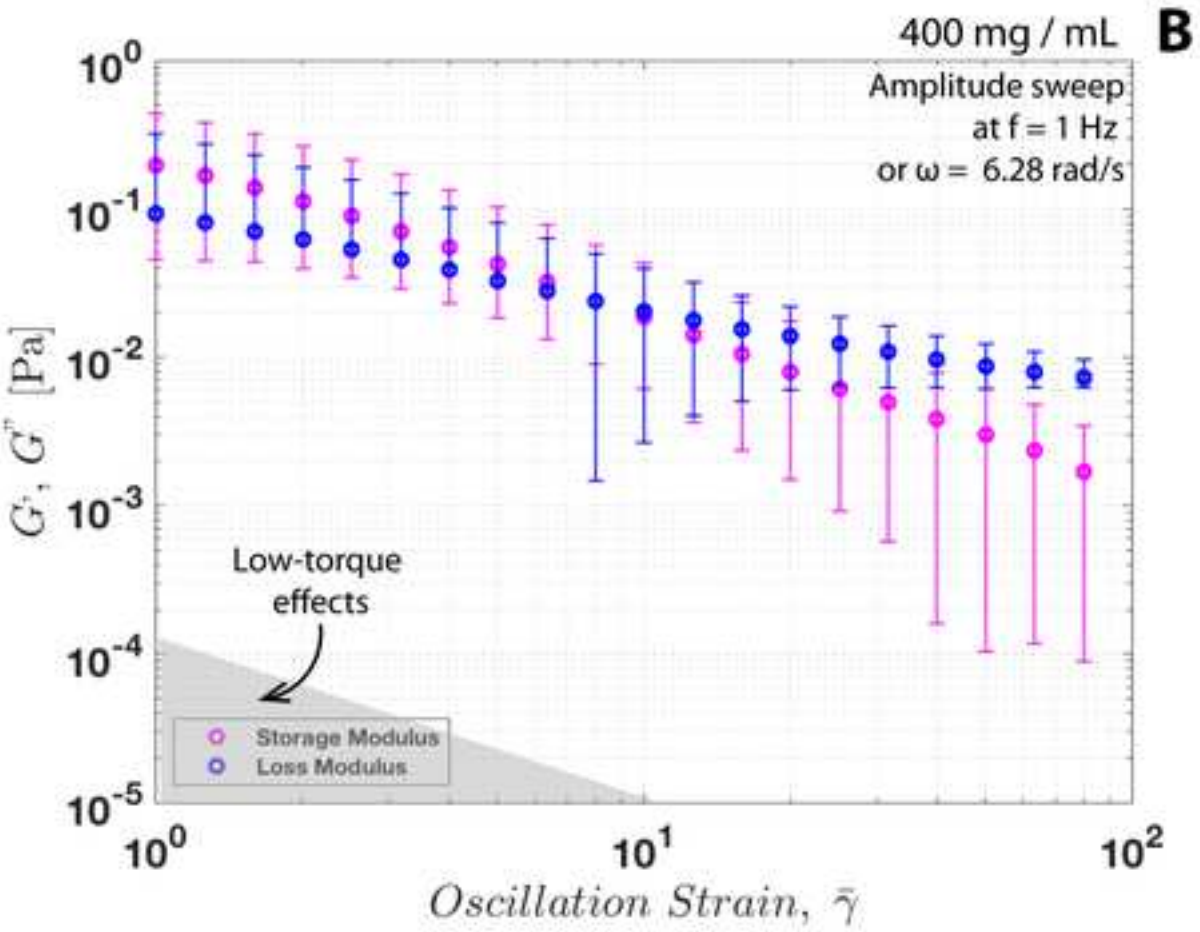

Figure7

Click here to access/download;Figure;Figure_7.tif

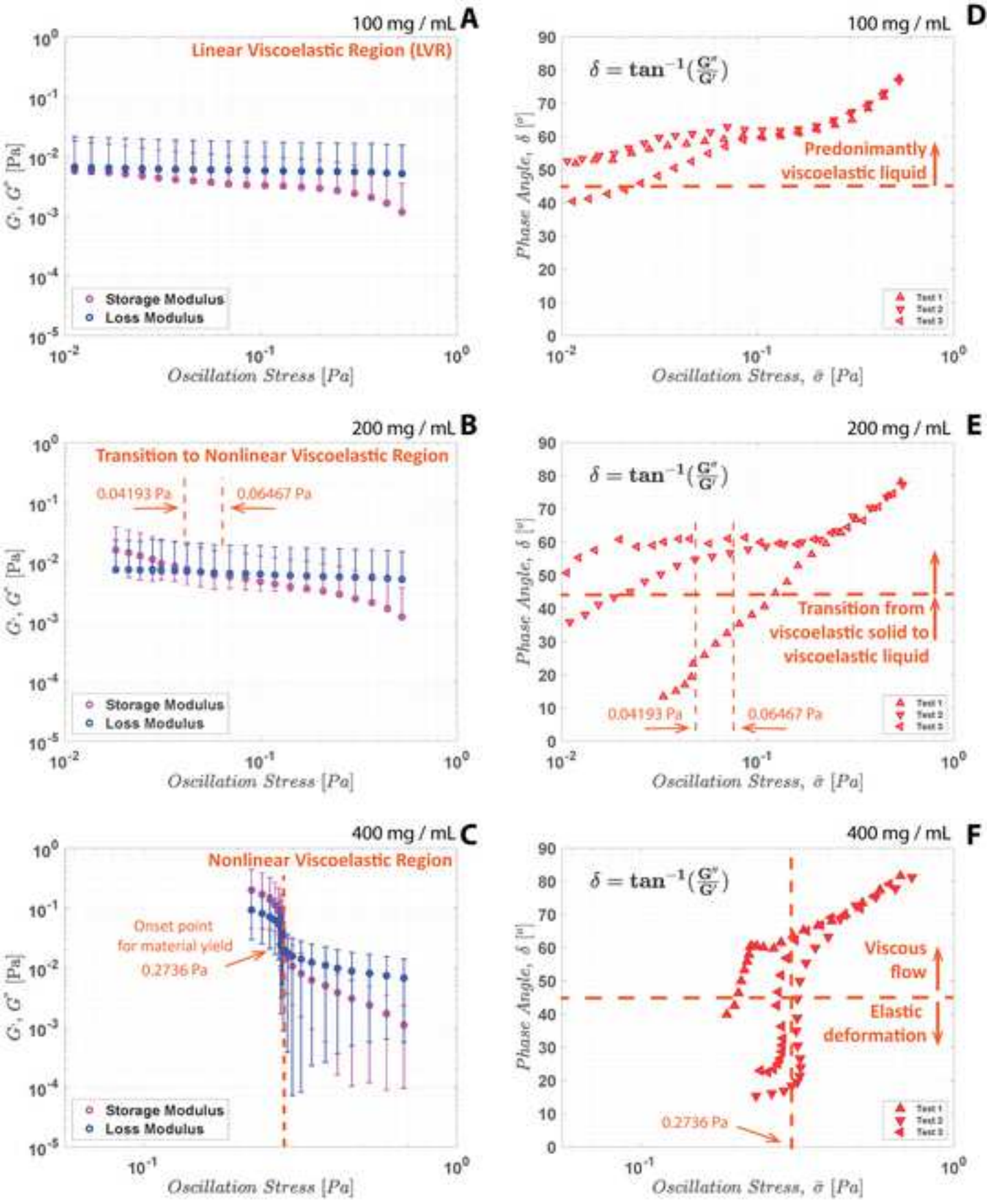

Figure8

Click here to access/download;Figure;Figure_8.tif

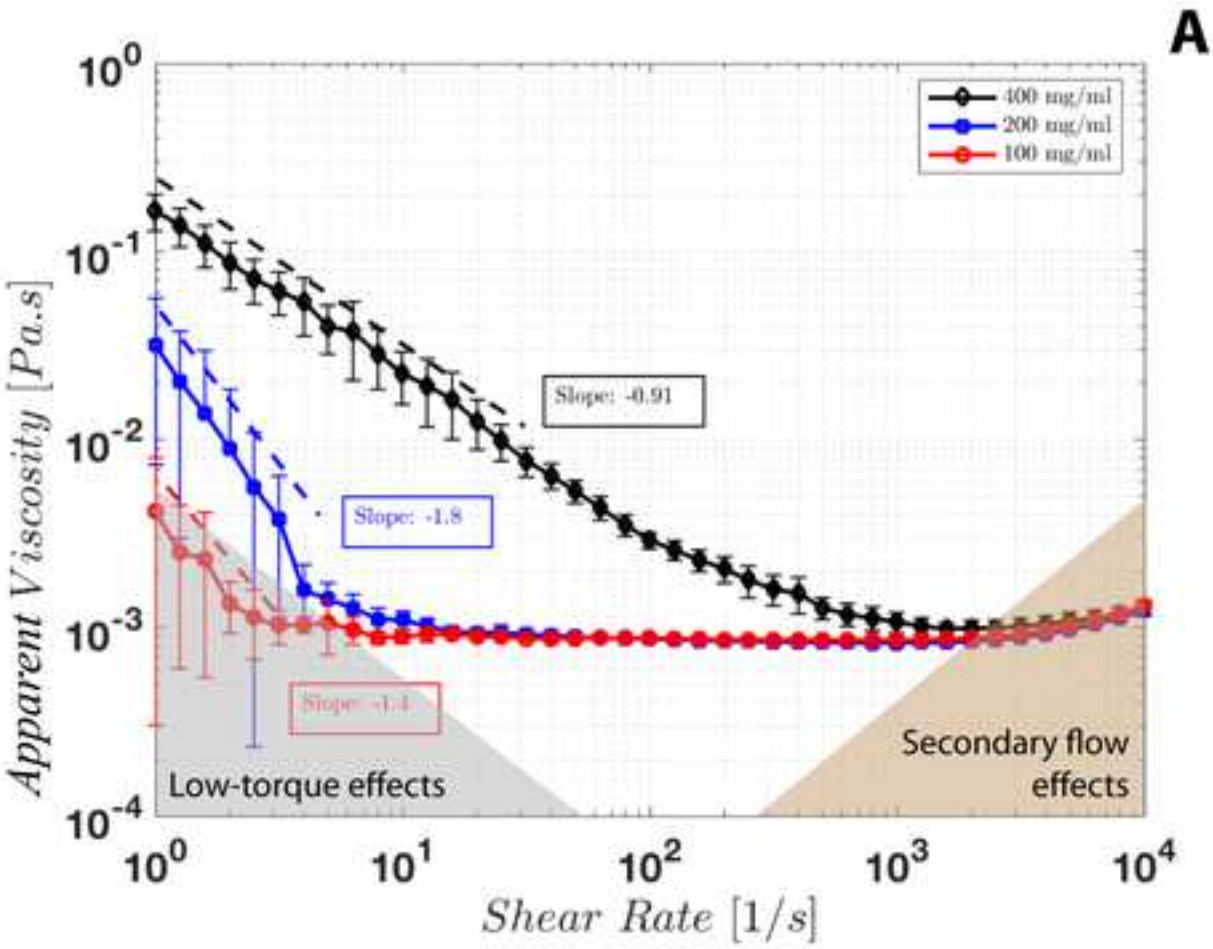

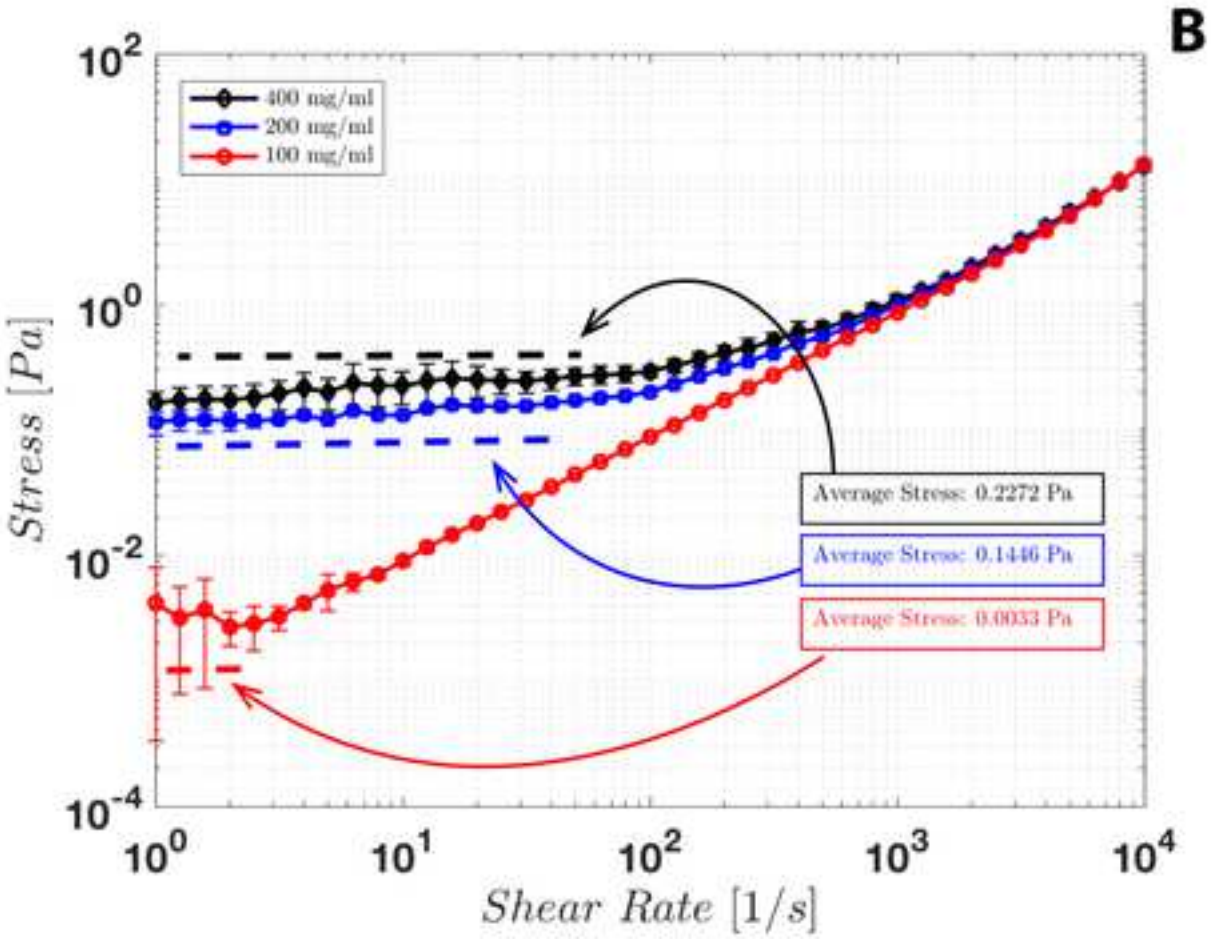

Click here to access/download;Table;Table 1.xlsx

Component	Model/Part No./Version
Rheometer	DHR-2
Geometry	513404.905
Peltier Plate	533210.901
Trios software	v4.5.042498
MATLAB Programming Language	R2017a

Parameter Description
Frequency Range
Maximum Angular Velocity
Minimum Torque under Steady shear
Minimum Torque under Oscillation
Maximum Torque
Torque Resolution
Shear Rate Range
Maximum Normal Force
Normal Force Resolution
Dimensions
Temperature Range
Measurement and analysis software
Data analysis, post-processing and graphical representation

Specifications
1 x 10−7 - 100 Hz
300 rad/s
10 nN.m
2 nN.m
200 μN *m
0.1 nN.m
5.73 x 10−6 to 1.72 x 104 [1/s]
50 N
0.5 mN
40 mm diameter 1° 0’ 11” Cone angle
-40°C to 200°C ± 0.1°C
n/a
n/a

Click here to access/download;Table of Materials;Table of materials.xlsx

Name	Company	Catalog
Materials		
Kim Wipes	VWR	470224-038
Gloves	VWR	89428-750
Pipette	VWR	89079-974
Pipette Tips	Thermo Scientific	72830-042
Shaker	VWR	89032-094
Vials	VWR	66008-710
Weigh Scale	Ohaus	Scout –SPX Balances
Chemical Reagents		
De-Ionized Water (H20)	-	-
Sterile 70% Isopropanol (C3H8O)	VWR	89108-162
GR Mucus		
100 mg/mL concentration, 2mL	-	-
400 mg/mL concentration, 1mL	-	-
200 mg/mL concentration, 1mL	-	-
Software		
MATLAB	Mathworks	R2017a
Trios	TA Instruments	v4.5.042498

Comments

To clean Sample from plate
To prevent contamination of sample
To transport sample from vial to rheometer
To transport sample from vial to rheometer
To homogenously mix sample of mucus
Contains measured sample volumes
To weigh mass of mucus samples
Liquid
Liquid

Viscoelastic Material
Viscoelastic Material
Viscoelastic Material

Data analysis, post-processing and graphical representation
Rheometer instrument control and analysis software

Rebuttal Letter

Click here to access/download;Rebuttal Letter;JoVE61379R1_RebuttalLetter_05272020.pdf

THE GEORGE WASHINGTON UNIVERSITY
WASHINGTON, DC

School of Engineering & Applied Science

Mechanical & Aerospace Engineering
Science and Engineering Hall
800 22nd Street, NW, Suite 3000
Washington, DC 20052

t 202 994 6749
f 202 994 0127
mueng@gwu.edu

May 27, 2020

Dr. Vineeta Bajaj,
Review Editor
JoVE (Journal of Visualized Experiments)
17 Sellers St.
Cambridge, MA 02139

Dear Dr. Bajaj,

We are submitting the revised manuscript titled "Macro-rheology characterization of gill raker mucus in the Silver Carp, *Hypophthalmichthys molitrix*," toward your consideration for publication in JoVE. In this revision, we addressed your comments and suggestions using "Track changes". Our detailed responses are also attached with this letter.

We look forward to hearing back from you regarding our manuscript.

Thank you for all your suggestions, as they improved the quality of our revised manuscript greatly.

.

Sincerely,

Kartik V. Bulusu, D.Sc.
Assistant Research Professor
Department of Mechanical and Aerospace Engineering
The George Washington University, Washington DC 20052
Phone: (202) 491 1084
Email: bulusu@gwmail.gwu.edu

Attachment: [Response to editorial comments]

Response to editorial comments

We thank the review editor for the suggestions and comments presented in the current review of our manuscript. Below we responded point-by-point to all the suggestions and comments made in the review. The editor's suggestions are marked in **'Times New Roman font'** *and our response follow in 'Calibri* font*'. The instances where text from the revised manuscript is included verbatim in this rebuttal, we present them using* 'Times New Roman font' *in our response. The revised manuscript has been put together with "Track Changes".*

1. **The manuscript needs a thorough proofreading.**

   Response:
   Thank you for suggesting a thorough proof-read in this revision. We made sure that there are no typographical and formatting errors in this revision.

2. **Abstract is made crisp, please check.**

   Response:
   We are grateful for the changes made in our abstract.

3. **Please remove the redundancy make the introduction crisp. This actually needs a good copyediting.**

   Response:

   We thank the review editor for the guideline on improving the introduction-section. We modified this section following the review editors' comment. Several typographical errors were fixed in this revision. The changes can be noticed in the revised manuscript using "Track changes". We took care to avoid redundancy by deleting repetitive words and phrases in this section. Further, any verbatim mention of sentences across the manuscript have been avoided. Complex sentences were broken down into small phrases so that the section can be made crisp and clear. We took care in reordering the references so that they are pointing to the citations accurately. The figures were also reordered to make sure they are correctly described in the revised text.

   Responses to the editor's specific comments are presented below:

   a. ***"The GR mucus properties investigated in the protocol using a strain rate controlled, rotational rheometer follow."*** **Follow what ?**

      Response:

      The sentence was modified to address the editor's concerns as presented below.

"The GR mucus properties investigated in the protocol using a strain rate controlled, rotational rheometer are described below."

b. ***"Increase in apparent viscosity would lead to a reduction in velocity of flowing liquid for any give pressure gradient?"***

Response:

The sentence was modified to address the editor's concerns, but we eventually deleted it as it was not relevant for describing Figures 3A and 3B.

c. ***"The GR mucus properties investigated in the protocol using a strain rate controlled, rotational rheometer follow."*** **Follow what? Test are performed to generate data pertaining to G' G' and n? Please revise and make crisp sentences throughout.**

Response:

The sentence was modified to address the editor's concerns as presented below.

"The types of rheometer tests performed to monitor data pertaining to storage modulus (G'), loss modulus (G") and apparent viscosity (η) are described below. The dynamic oscillation tests (strain sweeps and frequency sweeps) monitored G' and G" under controlled oscillation of cone geometry."

The following text has been included in the modified introduction-section:

"The silver carp, *Hypophthalmichthys molitrix*, is a planktivorous filter feeder and an invasive species that has infiltrated several natural waterways in the United States. This species was initially introduced in the upper Mississippi River basin to control algal blooms[1-3]. The silver carp is an extremely efficient feeder. Typically, its consumable food particle sizes range from 4 to 20 μm to larger zooplankton that are around 80 μm[3-5]. This species has outcompeted other native fish and can potentially cause enormous damage to native waterways by limiting available resources[1-2,6]. Thus, filter feeding fish such as the silver carp and the bighead carp pose a major threat to the Great Lakes[1-2,6-8].

Filter feeding fish possess special organs called the gill rakers (GRs) with a thin layer of mucus residing on their surface. These organs improve the efficiency of filtration and aggregation of small particles from the incoming fluid. The goal of the protocol presented herein is to characterize the non-Newtonian, shear thinning material property and yield stress of the GR mucus acquired from the inner surface of the gill rakers in the silver carp. The value of yield stress of the GR-mucus, ascertained using a rotational rheometer, is of interest. The measured yield stress is referred to as an "apparent yield stress" since it depends on the testing methods such as steady shear rate- or dynamic oscillatory strain-type[9-10]. Currently the most utilized rheological phenomenon is the shear-thinning 'yield-

stress fluid,' or the transition from solid-like to liquid-like behavior at a critical applied stress[9,11]. The apparent yield stress is the minimum shear stress required to initiate flow or that at which irreversible plastic deformation is first observed when the mucus transitions from a gel-like material to a fluid-like material. This behavior can be observed in structured viscoelastic materials such as the mucus layer on GRs. The transition from gel-like to fluid-like behavior of the GR mucus entails two functions i.e., an adhesive role to gather food particulates and a transport vehicle role to assist in the delivery and filtration process. The extended function of the mucus includes creating diffusion barriers in disease resistance and respiration, providing controlled release of nutritional factors, toxic components and excretion, metabolic pathways for feeding and nesting, predator protection, and boundary layer modification that improves the locomotion and propulsive efficiency[12-14].

Complex fluids like the mucus possess properties that vary with flow conditions and require additional measurement parameters to define their bulk scale physical behavior. To monitor the viscosity and yield stress of GR mucus, rheological measurements are performed using a rotational rheometer. The rotational rheometer applies a steady or oscillatory shear stress or strain by means of a rotating disk in contact with the fluid sample and measures its response. The rationale behind using this instrument and technique is that the rheometer can provide a set of measurements to describe the material properties of the GR mucus of the silver carp, which cannot be defined by viscosity alone.

The mucus is a viscoelastic material and its mechanical response to an imposed deformation is between that of a pure solid (governed by Hooke's law of elasticity) and that of a pure liquid (governed by Newton's law of viscosity)[15-16]. The complex macromolecular network contained within the mucus can stretch and reorient in response to external forces or deformation. A rotational rheometer is comprised of a cone geometry and a Peltier plate as shown in **Figures 1** and **2** (see **Table 1** for instrumentation specifications). The objective of this study was to develop a protocol to determine the rheological properties of the GR mucus. An advantage of the rotational rheometer over a viscometer is its ability to make dynamic measurements using small sample volumes. The GR mucus sample volume in this study was approximately 1.4 mL. The viscometer, on the other hand, is limited to constant shear rates and requires large sample volumes.

The rheological properties of the mucus are expected to vary greatly within the silver carp anatomy. For example, the rheological properties of the mucus residing on the inner GR surfaces may be different from that on the outer GR surfaces or the epibranchial organ. To account for the potential variability of mucus properties in different regions of the fish, the acquired GR mucus sample was diluted and solutions of various concentrations were created to develop an understanding of the variation in rheology. The rotational rheometer with cone geometry and a Peltier plate was then used in this protocol to investigate the various small samples of mucus. The data and results regarding mucus rheology reported after executing the protocol demonstrated the efficacy of the

measurement technique and were not meant to be generalized across the entire silver carp population. The protocol presented herein can be extended to investigate mucus rheology across larger sample sets to test other hypotheses.

The purpose of this study is to demonstrate the variation of rheological properties of GR mucus rheology with three different mucus concentrations (400 mg/mL, 200 mg/mL and 100 mg/mL). The 400 mg/mL concentration represents the raw mucus sample harvested from the fish GRs. Distilled water (DI) was used to dilute the raw mucus sample into 200 mg/mL and 100 mg/mL concentrations. Diluting the mucus samples allowed us to evaluate the extent of shear thinning and apparent yield stress as a function of concentration and to determine the concentration at which the GR mucus transitions to non-Newtonian behavior. A shaker was used to break down any large clumps of mucus in the samples to mitigate errors in the rheological data due to inhomogeneity.

In most vertebrates, including fish, the predominant mucus-forming macromolecules are glycoproteins (mucins) that tend to swell in water by entanglements or chemical cross-linking and create a gel-like material[12-13,17-20]. The high-molecular-weight gel-forming macromolecules and high-water content reflects the slipperiness in the mucus[13]. A high degree of inter-macromolecular interactions leads to gel-formation whereas lower levels of inter-macromolecular interactions or broken bonds result in high-viscosity fluids[21].

The processes of food particulate filtration in filter feeding fish are aided by GR mucus-related properties such as cohesion and viscosity that determine its potential toward adhesion and tack [22]. The strength of mucus-based adhesion depends on specific intermolecular interactions, electrostatic or hydrophobic interactions[23]. Sanderson et al.[24] conducted a suspension-feeding study in blackfish wherein they found the evidence for mucus-based adhesion. They stated that the adhesion of suspended food particulates with a mucosal surface is followed by the transport of aggregated clumps of particles bound together with mucus by directed water-flow acting on it[24]. Endoscopic techniques were used to observe filtered particles[24]. The mucus exposed to shear strain rates generated from water-flow facilitates the delivery of food particulates to digestive organs.

Literature on the range of shear rates and practical limits in the rheological testing of GR mucus is scarce. Therefore, guidance was sought from rheological studies on gastric, nasal, cervical and lung mucus, salmon skin mucus, hagfish slime, and bone-joint surface lubricant wherein the rheological characterization and non-Newtonian attributes of the mucus has been ascertained previously[11-12,25-31]. More recently, the effect of fish skin mucus on locomotion and propulsive efficiency has been studied using constant shear rate viscometry. Skin mucus rheology studies (without any dilution or homogenization) pertaining to seabream, sea bass and meagre demonstrated non-Newtonian behavior at typically low shear rates[14]. In another related study, the raw skin mucus samples from dorsal and ventral sides of the Senegalese sole were found to exhibit non-Newtonian behavior, indicating a higher viscosity of the ventral mucus at all shear rates considered[32].

Other rheological protocols pertaining to hydrogel scaffold development and for highly concentrated suspensions using a constant shear rate viscometer have also been reported in the literature[33-34].

The GR mucus properties investigated in the protocol using a strain rate controlled, rotational rheometer are described below. These properties describe the rheology of complex biological fluids [25]. For Newtonian fluids, the apparent viscosity remains constant and is shear-rate-independent and the shear stresses vary linearly with shear strain rates (**Figures 3A and 3B**). For non-Newtonian fluids (such as shear-thinning fluids) viscosity is shear-rate-dependent or deformation-history-dependent (**Figure 3A and 3B**). The loss modulus (G") represents the extent to which the material resists the tendency to flow and is representative of fluid viscosity (**Figure 4**). The storage modulus (G') represents the tendency of the material to recover its original shape following stress-induced deformation and is equivalent to elasticity (**Figure 4**). The phase angle (δ) or loss tangent value, is calculated from the inverse tangent of G"/G'. It represents the balance between energy loss and storage and is also a common parameter for characterizing viscoelastic materials (δ = 0° for a Hookean solid; δ = 90° for a viscous liquid; δ < 45° for a viscoelastic solid and δ > 45° for a viscoelastic liquid) (**Figure 4**) [25]. The apparent yield stress (σ_y) in structured fluids represents a change of state that can be observed in rheological data from steady state sweep and dynamic stress-strain sweeps[10]. If the external applied stress is less than the apparent yield stress, the material will deform elastically. When the stress exceeds the apparent yield stress (marked as "average stress" in **Figure 3B**), the material will transition from elastic to plastic deformation and begin to flow in its liquid state[35]. Measuring the storage modulus (G') and loss modulus (G") in the mucus-sample under oscillatory stress (or strain) conditions quantifies the change in the material state from gel-like to viscoelastic liquid-like behavior.

The types of rheometer tests performed to monitor data pertaining to storage modulus (G'), loss modulus (G") and apparent viscosity (η) are described below. The dynamic oscillation tests (strain sweeps and frequency sweeps) monitored G' and G" under controlled oscillation of cone geometry. The dynamic strain sweep tests determined the linear viscoelastic region (LVR) of the mucus by monitoring the intrinsic material response (**Figure 4**). Strain sweeps were used to determine the yielding behavior at constant oscillation frequency and temperature. The dynamic frequency sweep tests monitored the material response to increasing frequency (rate of deformation) at a constant amplitude (strain or stress) and temperature. Strain was maintained in the linear viscoelastic region (LVR) for the dynamic frequency sweep tests. The steady-state shear rate tests monitored the apparent viscosity (η) under steady rotation of the cone geometry. The GR mucus was subjected to incremental stress steps and apparent viscosity (η, Pa.s) was monitored for varying shear rate ($\dot{\gamma}$, $1/s$).

The protocol presented in this paper treats the GR mucus as a complex structured material of unknown viscoelastic nature with a certain linear viscoelastic response range.

The fish mucus was extracted from the GRs of the silver carp during a fishing expedition at the Hart creek location in the Missouri River[1-2,36]. An array of GRs inside the mouth of a Silver carp is shown in **Figure 5A** and a schematic drawing of the same is presented in **Figure 5B**. An excised GR is shown in **Figure 5C.** Extraction of mucus from GRs of the silver carp is summarized in the schematic drawings, **Figures 5D,E**. All the rheometer tests were performed under a constant, controlled temperature of 22 ± 0.002 °C, the temperature recorded at the fishing site[1-2,36]. Each mucus sample was tested three times with the rheometer, and the averaged results are presented in figures along with the statistical uncertainty bars."

4. **Please move all the softwares to the table of materials as these are commercial. [Comment on the note pertaining to protocol step-2]**

   Response:

   Thank you for mentioning the need for moving commercial nomenclature. We have now moved the commercial software information into the table of materials as suggested. We also combined tables 2 and 3, into one table of materials following the comment #8 below.

5. **"Perform these steps on the samples individually." Added here, please check. [Comment on protocol step-2.8]**

   Response:

   Thanks for the suggestion. We updated the sentence to make sure it fits our protocol step as presented below.

   "Perform these steps on the available mucus concentration samples individually."

6. **Steps 2.8.13 – 2.8.15 – Redundant, please remove**

   Response:

   Thank you for mentioning the redundancy of steps 2.8.13 – 2.8.15. We have removed them from the manuscript.

7. **[Comment on the discussion-section first paragraph]** ***"Our objective in using this technique and protocol is to establish that it is well-suited for further investigation with larger mucus sample volumes. We acknowledge that more samples from a school of silver carp would need to be analyzed to fully characterize the rheological properties of the GR mucus and the data presented herein is not a generalization across the silver carp population. Our technique is justified due its efficacy with rheological characterization of mucus when small volumes are available."*** **This can be moved to the discussion.**

Response:

Thank you for the suggestion to move the sentences to the discussion-section. We agree that it fits better in the discussion-section and followed the suggestion. These sentences are now the first paragraph of the discussion-section. The updated discussion-section is presented as our response to comment #10 below.

8. **FIGURE AND TABLE LEGENDS – Chemicals, instruments, and reagents, buffers, etc should be combined into one table of materials. The table should include the name, company, and catalog number of all relevant materials in separate columns in an xls/xlsx file.**

Response:

Table 2 and 3 from the previous revisions are combined into one table of materials as suggested in comment #4 and #8. We updated the table of materials with the information to the best of our knowledge and hope that they are now looking complete.

   a. **Table 2: List of Chemical Reagents Used – Table 2 is not the chemical reagents used?**

Response:

We hope that the updated table of materials can make things clearer. Thank you for the suggestion.

9. ***"Supplementary Figure 5: Gap Options Page. The gap tab is used to set how the rheometer will zero the distance between the geometry and plate. Specifically, an axial force of 1N will be used to gage where zero distance is***." **- ????**

Response:

The caption and the description are modified to make the Supplementary Figure 5 clear.

"Supplementary Figure 5: Measurement Gap Options The **"**gap" tab options are accessed to set the conditions for zero gap mode and traverse velocity of the measurement head. An axial contact force between the geometry and the Peltier plate was set to 1 Newton to ensure the zero-gap reference, i.e., the contact between cone geometry and the surface of the Peltier plate. The measurement head can then be made to accurately traverse to the measurement gap of 28 µm between the 40 mm 1° cone geometry and the Peltier plate."

10. DISCUSSION – Please make the discussion crisp and remove redundancy throughout.

Response:

We thank the review editor for the guideline on improving the discussion-section. We modified this section following the review editors' comment. The first paragraph from the Representative results-section was moved as suggested in Comment #7. The portions that were redundant or repetitive after the results-section were removed.

The critical steps within the protocol, a modification of the protocol, suggested improvements, limitations and significance of the protocol are presented in separate paragraphs to ensure that the audience can peruse through them.

We discussed the physical insights from the GR mucus rheology data by reviewing schematic drawings presented in the Figures 3 and 4, so that the audience can easily understand the data trends and incorporate the approach presented in our protocol in future experiments.

One of the main points we made in this section is the need to review data that can be unsuitable for extended analysis. We felt this is an important point when working with very small sample volumes like the GR mucus and complex biological fluids. We cited papers by Nelson and Ewoldt (2017) and Ewoldt et al. (2015) that discuss instrumentation limitations, low-torque effects and secondary flow effects in detail.

The data we presented by the successful execution of the protocol were of high fidelity. The future users of this protocol can benefit from the discussion. The following text has been included in the modified discussion-section:

"One of the main objectives of developing this protocol is to establish that it is well-suited for rheological characterization of GR mucus when very small sample volumes are available. We acknowledge that more samples from a school of silver carp would need to be analyzed to fully characterize the rheological properties of the GR mucus and the data presented herein are not a generalization across the silver carp population. Our technique is justified due its efficacy with rheological characterization of small sample volumes and can be used in extended investigations with larger mucus sample volumes***.***

The critical steps within the protocol are the preparation of mucus solutions of various concentrations, measurements and data acquisition using a rotational rheometer, and graphical representation and data analysis for physical insights.

Physical insights into GR mucus data are drawn from schematic representations shown in Figures 3 and 4, that are annotated with attributes of the expected material behavior. **Zero-shear strain rate viscosity** (η_o) values can be observed at low-shear strain rates where mobility of the material molecules dominates (Figures 3A and 8A). **Infinite-shear strain viscosity** (η_∞) values in non-Newtonian fluids are orders of magnitudes lower than the zero-shear strain rate viscosity. These data can be noticed at high shear rates where

there is little or no dependence on intermolecular interactions (Figures 3A and 8A). For non-Newtonian fluids, apparent viscosities progressively decrease as the shear rates increase and attain a constant low value (Figures 3A and 8A). **Yielding behavior in the GR mucus under steady state measurements** can be represented with slope as shown in Figure 3A and presented in Equation 1., where η_a represents the apparent viscosity, σ_y is the (constant) yield stress and $\dot{\gamma}$ is the shear strain rate.

$$\eta_a = \frac{\sigma_y}{\dot{\gamma}} \tag{1}$$

Figures 3A and 8B are presented on a log-log scale and therefore, Equation 1 attains the following form:

$$log\ \eta_a = k - \log \dot{\gamma} \tag{2}$$

where k – represents the apparent yield stress. On a log-log scale, the apparent viscosity decreases with a slope of '-1' indicating material yield as shown in Figure 3A [10]. The 200 mg/mL and 400 mg/mL mucus concentrations possessed slopes of -1.8 and -0.91, respectively, and demonstrate yielding behavior (Figure 8A). Under dynamic oscillation measurements, the viscoelastic characteristics are independent of the strain amplitude in the Linear Viscoelastic Region (LVR) (Figure 4). The **yielding behavior in the GR mucus under dynamic oscillation measurements** can be observed as the viscoelastic material (GR mucus) enters the non-linear viscoelastic region (NLVR) as the storage modulus (G') decreases (Figure 4). In the NLVR regime the viscoelastic material will demonstrate solid-gel-like behavior if the storage modulus is greater than the loss modulus (G' > G"). When the loss modulus exceeds the storage modulus (G' < G"), a "crossover" between G' and G" data occur. As shown in Figures 7B-C, the 200 mg/mL and 400 mg/mL GR mucus concentrations demonstrated fluid-like behavior marked by the "crossover" between G' and G" data. The **apparent yield stress under steady state measurements** is represented as the average value of stress until an inflection point is reached (Figure 3B). Thereafter, the stress begins to increase sharply with an increase in the shear strain rate as shown in Figures 3B and 8B. The GR mucus data (200 mg/mL and 400 mg/mL concentrations) showed shear-thinning fluid behavior until the material begins to yield (Figure 8A and 8B). The apparent yield stress was observed clearly in 200 mg/mL and 400 mg/mL mucus concentrations due to their non-Newtonian characteristics (Figures 8B). The **apparent yield stress under dynamic oscillation measurements** are shown in Figures 4 and 7A-C as the "crossover" region between G' and G" data, followed by G" values exceeding G'. The 400 mg/mL GR mucus data showed shear-thinning, non-Newtonian behavior. The onset point of material yield was observed with an apparent yield stress of approximately 0.2736 Pa (Figure 7C). The **hydrogel-to-fluid like transition** with phase angle ($\delta = \tan^{-1}$ (G"/G')) changes are presented in Figures 4 and 7D-F. The extrema in the phase angle is associated with a Hookean solid at 0° and viscous fluid at 90° as shown in Figure 4. The phase angle values around 45° were attributed to transition of gel-like behavior of the material to a fluid-like behavior. The 400 mg/mL mucus concentration clearly showed a

change in the material characteristic from hydrogel to fluid like behavior through the process of yielding with an apparent yield stress of ~ 0.2736 Pa (Figure 7F).

Understanding the measurement limitations and avoiding data unsuitable for physical interpretation is a challenge with complex and soft biological fluids, especially when working with small sample volumes[11]**.** The data generated under low-torque and secondary flow effects are unsuitable for physical interpretation and are dependent on the geometry used in the rheometer (such as cone and plate in this study). These regimes were identified to avoid any misrepresentation of experimental data suffering from instrument resolution and measurement artifacts due to momentum diffusion. **Low-torque limits** (Figures 5B and 8A) are functions of geometry and minimum torque generated by the instrument (Table 1). Under steady shear measurement conditions, the criterion for rejecting data affected by the low-torque limit for a cone-plate geometry of radius (R) with minimum torque (T_{min} = 10 x 10^{-9} Nm, Table 1) has been discussed by Ewoldt et al., (2015) and is presented below [11]:

$$\eta > \frac{\left(\frac{3}{2\pi R^3}\right) T_{min}}{\dot{\gamma}} \tag{3}$$

where $\dot{\gamma}$ is the shear strain rate. The regimes of instrumentation limitation governed by low-torque and secondary flow effects are marked in Figures 6A and 8A. Unlike the 100 mg/mL GR mucus concentrations, the 200 mg/ml and 400 mg/mL GR mucus concentrations were unaffected by low-torque effects clearly demonstrate non-Newtonian, shear thinning behavior with high zero-shear strain rate viscosities at low shear strain rates. The criterion for minimum measurable viscoelastic moduli under dynamic oscillation measurements has been discussed by Ewoldt et al**.,** (2015) and presented below (Equation 4) [11]**.** In Equation 4, for a cone-plate geometry of radius (R) the minimum torque under oscillatory shear (T_{min} = 2 x 10^{-9} Nm, Table 1).

$$G_{min} = \frac{\left(\frac{3}{2\pi R^3}\right) T_{min}}{\gamma_0} \tag{4}$$

where G_{min} is the storage modulus (G') or loss modulus (G") and γ_0 is the shear strain rate. The regimes of instrumentation limitation governed by low-torque effects are marked in Figures 6A and 6B. The **secondary flow regime under steady state measurements** is governed by an inward momentum diffusion of the fluid by means of an eddy residing within the rotational cone and plate geometry[11]**.** The secondary flow pattern increases torque incorrectly making the fluid appear to be shear-thickening (Figure 8A). The secondary flow limit in Figure 8A was drawn using the following relation:

$$\eta > \frac{L^3/R}{Re_{crit}} \rho \dot{\gamma} \tag{5}$$

where L = βR, β is the cone angle, R is the cone radius, ρ = 1000 kg m^{-3}, Re_{crit} = 4 and $\dot{\gamma}$ is the shear rate. This regime helped in the accurately estimating the infinite-shear strain viscosity (η_∞) values in GR mucus samples.

A modification of the protocol can be made by using a flat-plate geometry instead of the cone-plate geometry as shown in protocol presented herein. The flat-plate tests should be performed with a parametric variation of the measurement gap in the rotational rheometer to reveal the dependence of apparent yield stress on the measurement gap and geometry. The **suggested improvements** of the protocol presented in this paper are described below. A parametric variation of the strain amplitude in the linear viscoelastic regime (LVR) and oscillation frequency should be performed. 'Tack and peel' rheology tests should be performed to develop a full understanding of the adhesivity of the GR mucus. Rheology characteristics of GR mucus should be performed on larger sample volume ensembles along with studies to measure any traces of blood cells to account of its effect on the overall GR rheological properties.

The limitations of the protocol are described below. The intricacies of the GR mucus extraction-procedures and the presence of blood cells or tissue fragments in the mucus samples may influence the rheology of the mucus. However, it should be noted the mucus used in the protocol did not have any visible traces of blood. The GR mucus sample is a heterogenous material and can possess different rheological properties due to the variance in location of and the conditions post-extraction. This limitation was addressed by sufficiently homogenizing the GR mucus using a shaker to breakdown any large clumps of mucus and tissue presence. Another important limitation is the very small GR mucus sample volumes (approximately 1.4 mL) that can be harvested for analyses that constrain a generalization of GR mucus properties.

The significance of this protocol is that it allows for an accurate rheological characterization of non-Newtonian, biological fluids such as the mucus. The protocol presented herein paves the way for investigating other similar biological fluids associated with human, animal and plant secretions. In addition, synthetic fluids or polymer-based solutions that are analogs of biological fluids can be testing using this protocol to understand material properties under varying stresses, oscillation frequencies, and temperature. The protocol is well-suited for rheological characterization of biological fluids when very small sample volumes are made available."

11. The text mentions about 36 citations, please check. Please also see that citation number and references corresponds to each other.

Response:

Thank you for pointing this out. The missing reference was identified and included in the revised manuscript. Due the nature of changes made in the introduction- and discussion-

sections the citation numbering of the references were also checked and we feel that they are now complete.

The full list of 36 references are included below:

1. Cohen, K.E., Hernandez, L.P. The complex trophic anatomy of silver carp, *Hypophthalmichthys molitrix*, highlighting a novel type of epibranchial organ. *Journal of Morphology*. 279,1615–1628, (2018).
2. Cohen, K.E., Hernandez, L.P. Making a master filterer: Ontogeny of specialized filtering plates in silver carp (*Hypophthalmichthys molitrix*). *Journal of Morphology.* 279,925–935., (2018).
3. Cremer, M. and Smitherman, R. Food habits and growth of silver and bighead carp in cages and ponds. *Aquaculture*. 20(1), 57–64, (1980).
4. Battonyai, I. et al. Relationship between gill raker morphology and feeding habits of hybrid bigheaded carps (*Hypophthalmichthys spp.*). Knowledge and Management of Aquatic Ecosystems. 416,36, (2015).
5. Zhou, Q., Xie, P., Xu, J., Ke, Z., Guo, L. Growth and food availability of silver and bighead carps: Evidence from stable isotope and gut content analysis. Aquaculture Research. 40(14), 1616–1625, (2009).
6. Freedman, J. A., Butler, S. E., Wahl, D. H. Impacts of invasive Asian carps on native food webs (Final Report). Urbana-Champaign, IL: University of Illinois, Kaskaskia Biological Station. (2012).
7. Nico, L., Fuller, P., Li, J. Silver carp (*Hypophthalmichthys molitrix*)—FactSheet. (2017).
8. Walleser, L., Howard, D., Sandheinrich, M., Gaikowski, M., Amberg, J. Confocal microscopy as a useful approach to describe gill rakers of Asian species of carp and native filter-feeding fishes of the upper Mississippi River system. *Journal of Fish Biology*. 85(5), 1777– 1784 (2014).
9. Nelson, A. Z., Ewoldt, R. H. Design of yield-stress fluids: a rheology-to-structure inverse problem. *Soft Matter*. 13, 7578—7594, (2017).
10. Chen, T. Rheological Techniques for Yield Stress Analysis. TA Instruments Applications Note, RH025 (2020).
11. Ewoldt, R.H., Johnston, M.T., Caretta, L.M. Experimental challenges of shear rheology: how to avoid bad data. in: S. Spagnolie (Editor), Complex Fluids in Biological Systems, Springer, (2015).
12. Thornton, D. J., Sheehan, J. K. From Mucins to Mucus: Toward a more coherent understanding of this essential barrier. *Proceedings of the American Thoracic Society*. Vol 1, 54 – 61, (2004).
13. Shepard, K.L. Functions for fish mucus. *Reviews in Fish Biology and Fisheries*. 4, 401-429, (1994).
14. Fernández-Alacid, L., et al. Skin mucus metabolites in response to physiological challenges: A valuable non-invasive method to study teleost marine species. *Science of the Total Environment.* 644, 1323-1335, (2018).

15. Wagner, C.E., Wheeler, K.M., Ribbeck, K. Mucins and Their Role in Shaping the Functions of Mucus Barriers. *Annu. Rev. Cell Dev. Biol.* 34,189–215, (2018).
16. Bird, R.B., Armstrong, R.C., Hassager O. *Dynamics of Polymeric Liquids, Volume 1: Fluid Mechanics*. New York: Wiley. 1,255–84, (1987). Silberberg, A. Mucus glycoprotein, its biophysical and gel forming properties. *Symp. Soc. Exp. Biol.* 43, 43-64, (1989).
17. Mantle, M., Allen, A. Isolation and characterisation of the native glycoprotein from pig small intestinal mucus. *Biochem. J.* 195, 267-75, (1981).
18. Allen, A., Hutton, D.A., Pearson, J.P., Sellers, L.A. Mucus glycoprotein structure, gel formation and gastrointestinal mucus function. In Nugent, J. and O'Connor, M., eds. *Mucus and Mucosa* (Ciba Foundation Symposium). London: Pitman, 137-56, (1984).
19. Asakawa, M. Histochemical studies of the mucus on the epidermis of eel, *Anguillajaponica. Bull. Jap. Soc. Scient. Fish.* 36, 83-7, (1970).
20. Fletcher, T.C., Jones, R., Reid, L. Identification of glycoproteins in goblet cells of epidermis and gill of plaice *(Pleuroneces platessa* L.), flounder *(Platichthys flesus* (L.)) and rainbow trout (Salmo *gairdneri* Richardson). *Histochemical* J. 8, 597-608, (1976).
21. Silberberg, A. Mucus glycoprotein, its biophysical and gel forming properties. *Symp. Soc. Exp. Biol.* 43, 43-64, (1989).
22. Hills, B. *The Biology of Surfactants.* Cambridge: Cambridge Univ. Press. 408, (1988).
23. Aubert, H., Brook, A.J., Shephard, K.L. Measurement of the adhesion of a desmid to a substrate. *Br. Phycol.* J. 24, 293-5, (1989).
24. Sanderson, S.L., Cech, J.J., Patterson, M.R. Fluid dynamics in suspension feeding black fish. *Science.* 251, 1346-8, (1991).
25. Lai, S.K., Wang, Y.Y., Wirtz, D., Hanes, J. Micro- and macrorheology of mucus. *Advanced Drug Delivery Reviews*. 61(2), 86-100, DOI: 10.1016/j.addr.2008.09.012, (2009).
26. Chaudhary, G., Ewoldt, R.H., Thiffeault, J.L. Unravelling hagfish slime. *J. R. Soc. Interface.* 16, (2019).
27. Downing, S., Salo, W., Spitzer, R., Koch, E. The hagfish slime gland: a model system for studying the biology of mucus. *Science.* 214, 1143–1145, (1981).
28. Hwang, S.H., Litt, M., Forsman, W.C. Rheological properties of mucus. *Rheologica Acta*, Band 8, Heft 4, (1969).
29. Litt, M. Mucus rheology. *Arch Intern Med.* 126, 417 – 423, (1970).
30. Quarishi, M.S., Jones, N.S., Mason, J. The rheology of nasal mucus: a review. *Clin. Otolaryngol.* 23, 403 – 413, (1998).
31. Nordgård, C.T., Draget, K.I, Seternes, T. Rheology of salmon skin mucus. *Annual Transactions - The Nordic Rheology Society.* 23, (2015).
32. Fernández-Alacid, L., et al. Comparison between properties of dorsal and ventral skin mucus in Senegalese sole: Response to an acute stress. *Aquaculture*. 513, (2019).
33. Yüce, C., Willenbacher, N. Challenges in Rheological Characterization of Highly Concentrated Suspensions — A Case Study for Screen-printing Silver Pastes. *J. Vis. Exp.* 122, (2017).
34. Sultan, S., and Mathew, A. P. 3D Printed Porous Cellulose Nanocomposite Hydrogel Scaffolds. *J. Vis. Exp.* 146, (2019).

35. Barnes, H.A., Hutton, J. F., Walters, K. *An Introduction to Rheology*. Amsterdam: Elsevier, (1989).
36. "National Water Information System." *USGS Current Conditions for USGS 06910450 Missouri River at Jefferson City, MO*, U.S. Geological Survey, https://nwis.waterdata.usgs.gov/usa/nwis/uv/?cb_00010=on&cb_00060=on&cb_00065=on&format=gif_default&site_no=06910450&period=&begin_date=2018-09-19&end_date=2018-09-21.

We sincerely hope that the review editor will find the revisions made in the manuscript in agreement with the suggestions and that this work is meritorious for publication in the Journal of Visualized Experiments.

Supplemental File (Figures, Permissions, etc.)

Click here to access/download;Supplemental File (Figures, Permissions, etc.);Supplementary_Figure1.tiff

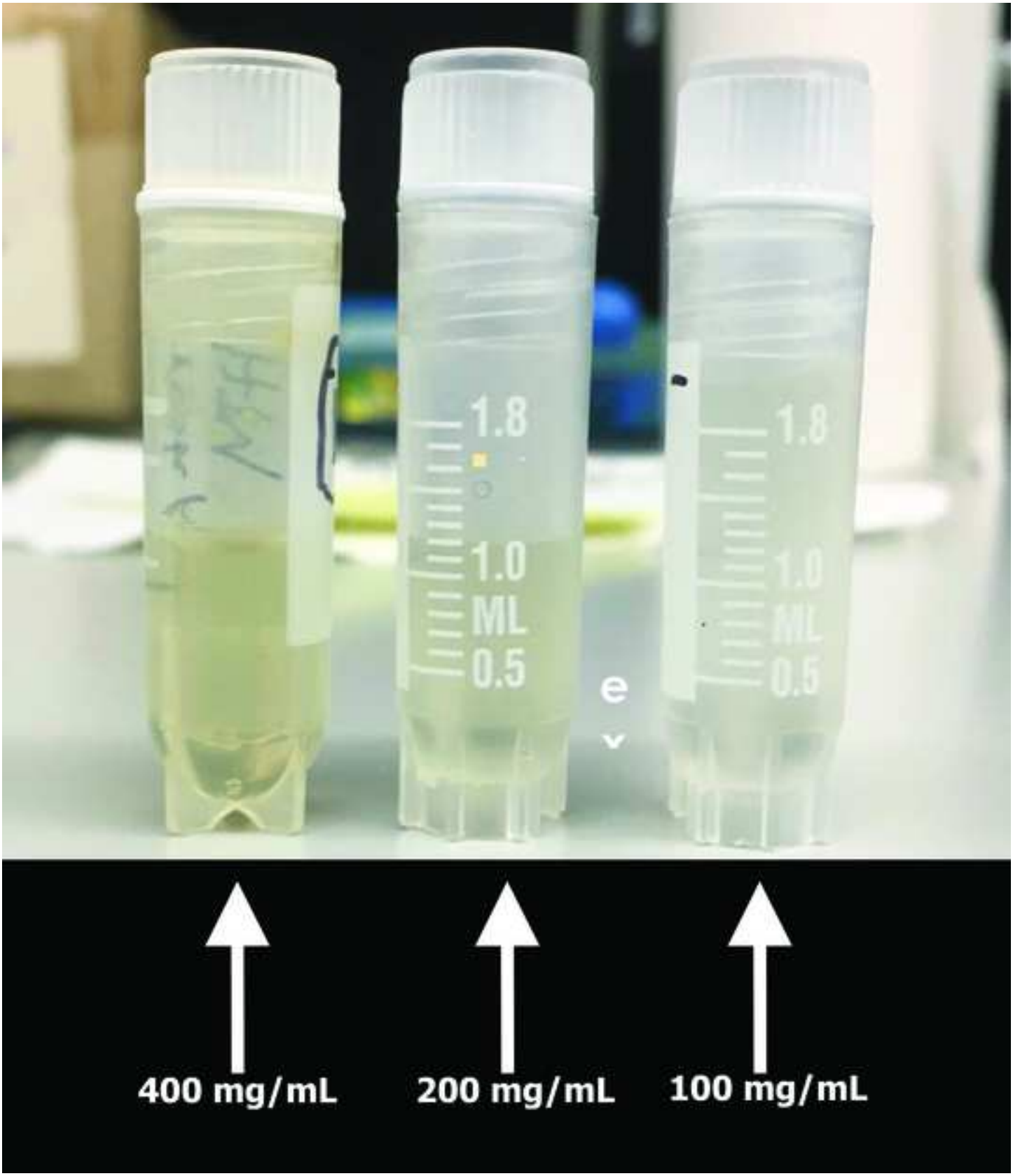

Supplemental File (Figures, Permissions, etc.)

Click here to access/download;Supplemental File (Figures, Permissions, etc.);Supplementary_Figure2.tiff

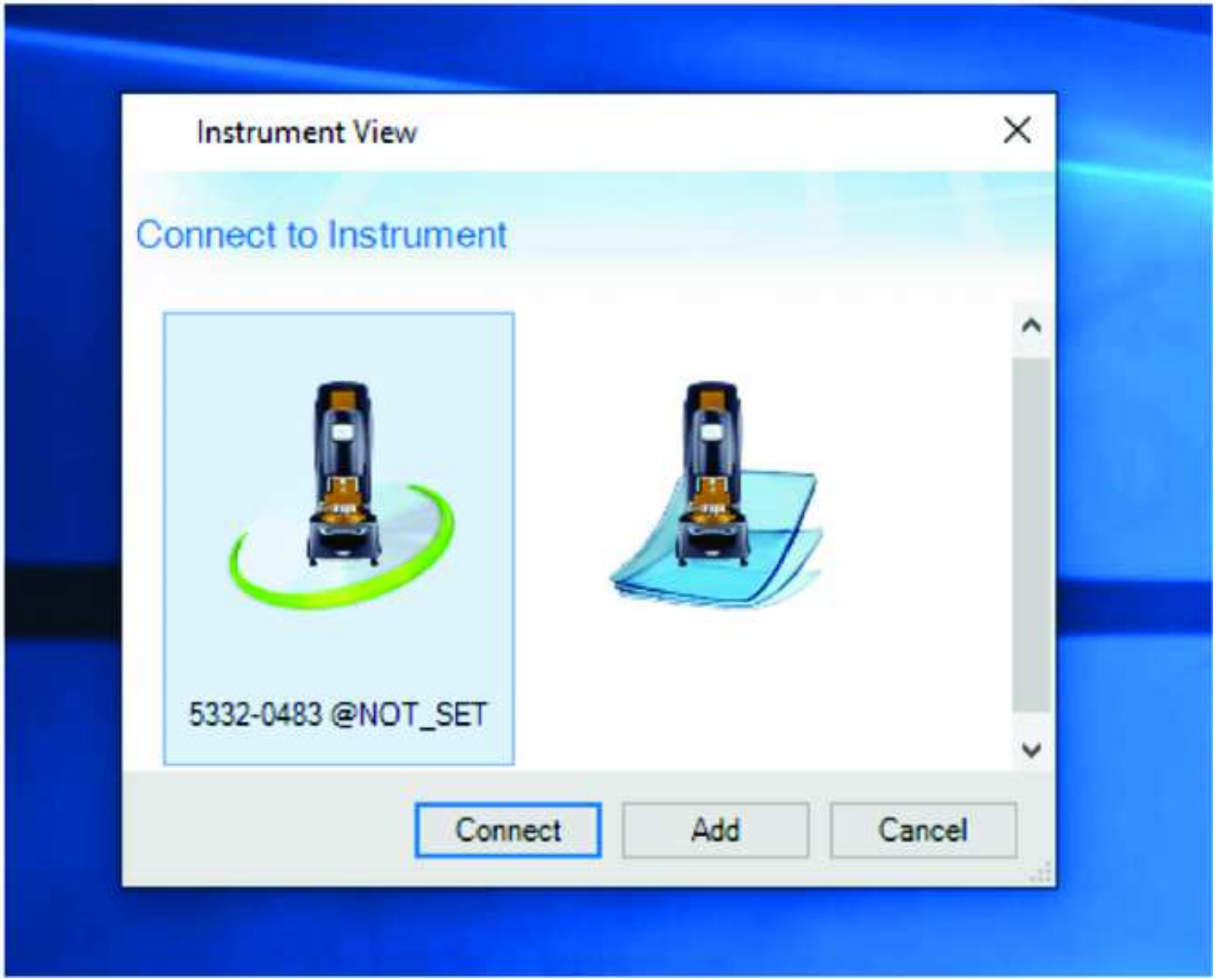

Supplemental File (Figures, Permissions, etc.)

Click here to access/download;Supplemental File (Figures, Permissions, etc.);Supplementary_Figure3.tiff

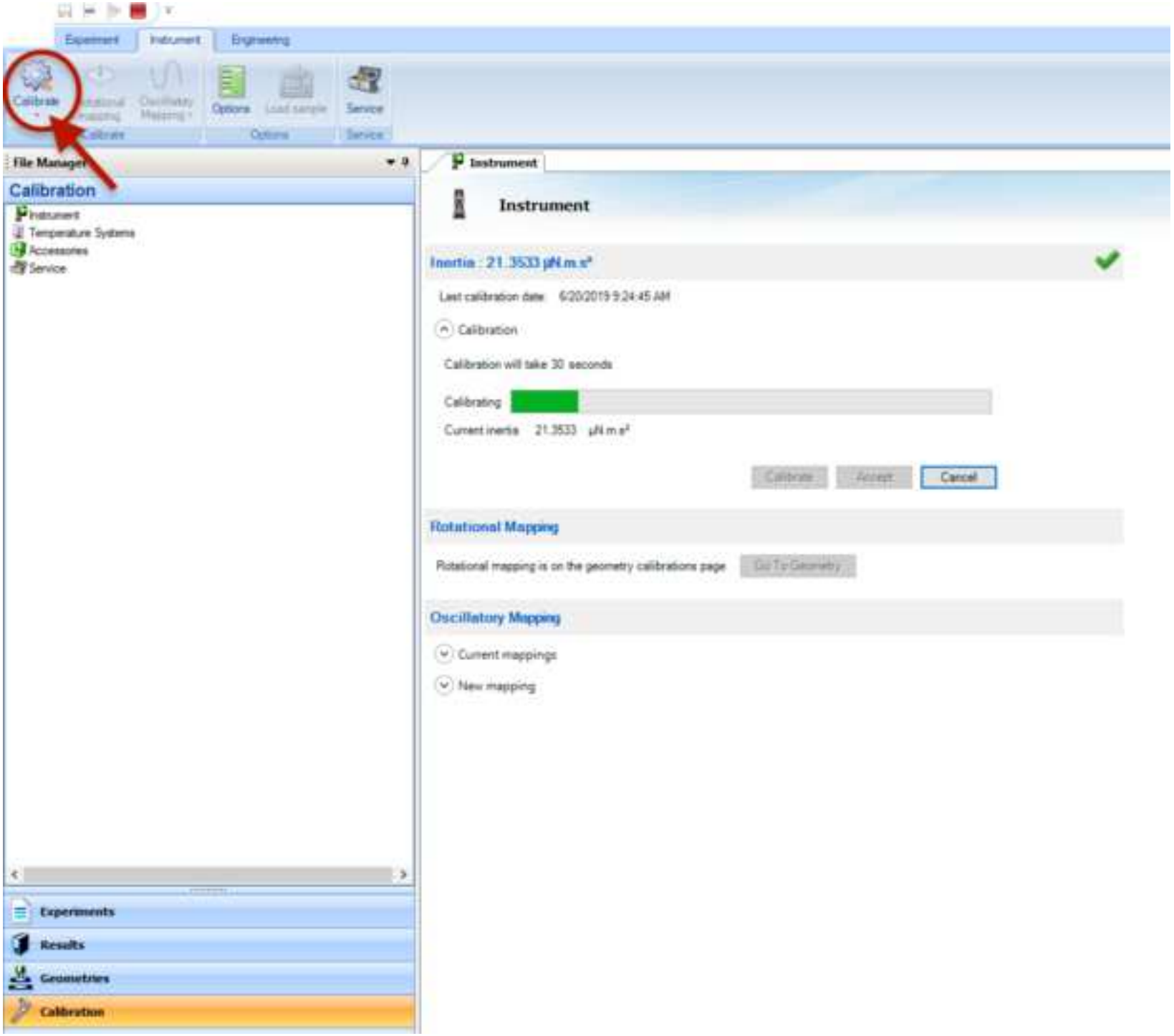

Supplemental File (Figures, Permissions, etc.)

Click here to access/download;Supplemental File (Figures, Permissions, etc.);Supplementary_Figure4.tiff

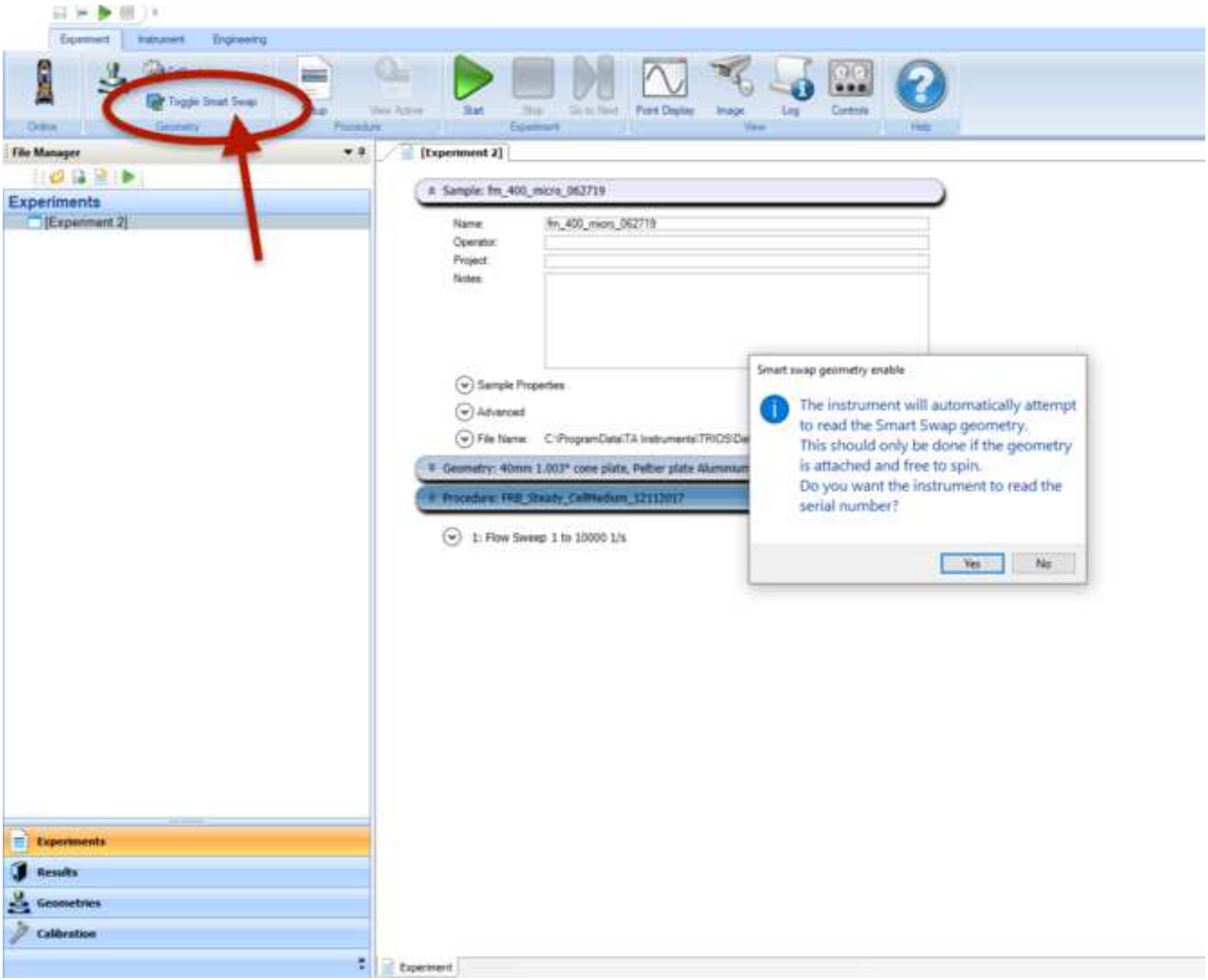

Supplemental File (Figures, Permissions, etc.)

Click here to access/download;Supplemental File (Figures, Permissions, etc.);Supplementary_Figure5.tiff

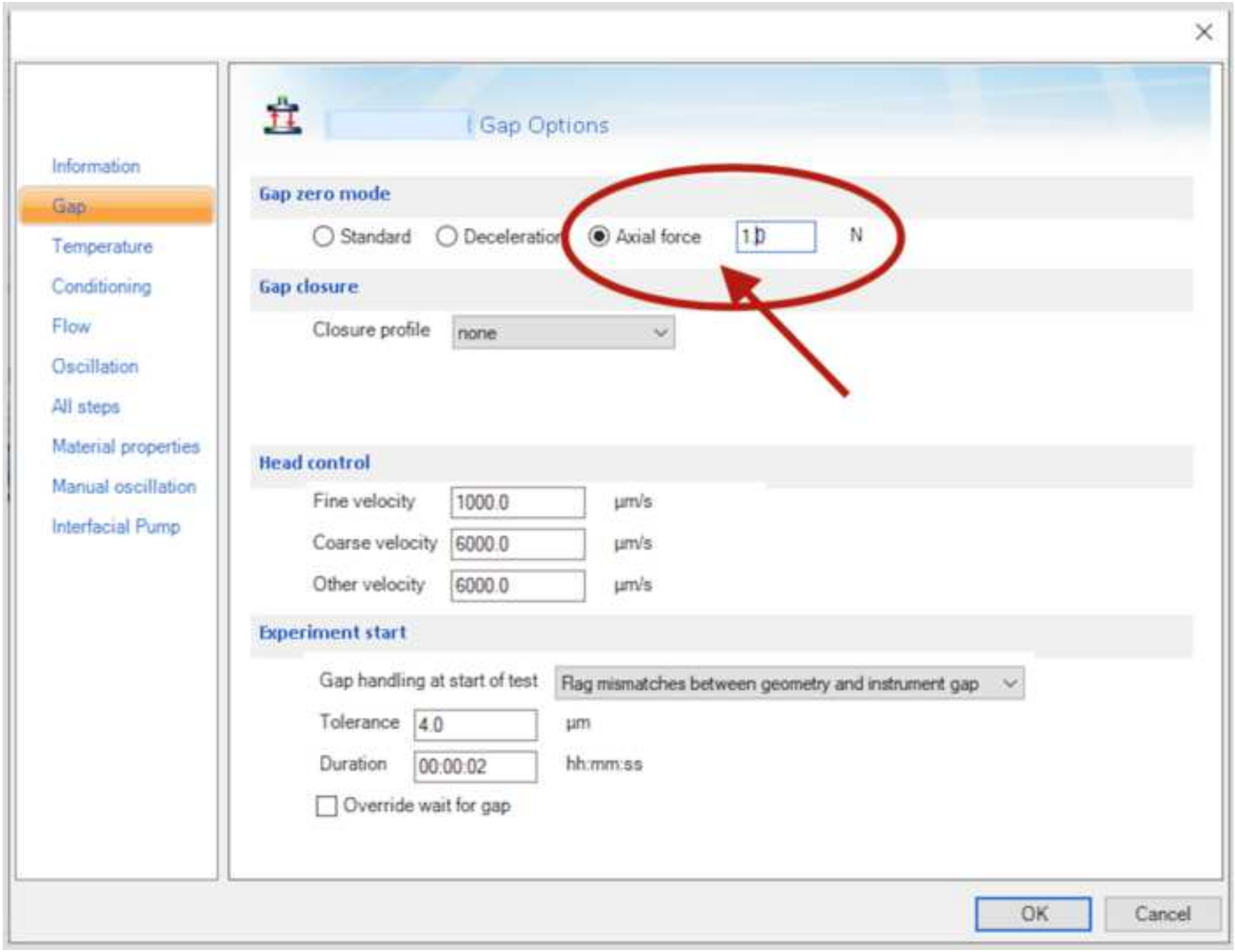

Supplemental File (Figures, Permissions, etc.)

Click here to access/download;Supplemental File (Figures, Permissions, etc.);Supplementary_Figure6.tiff

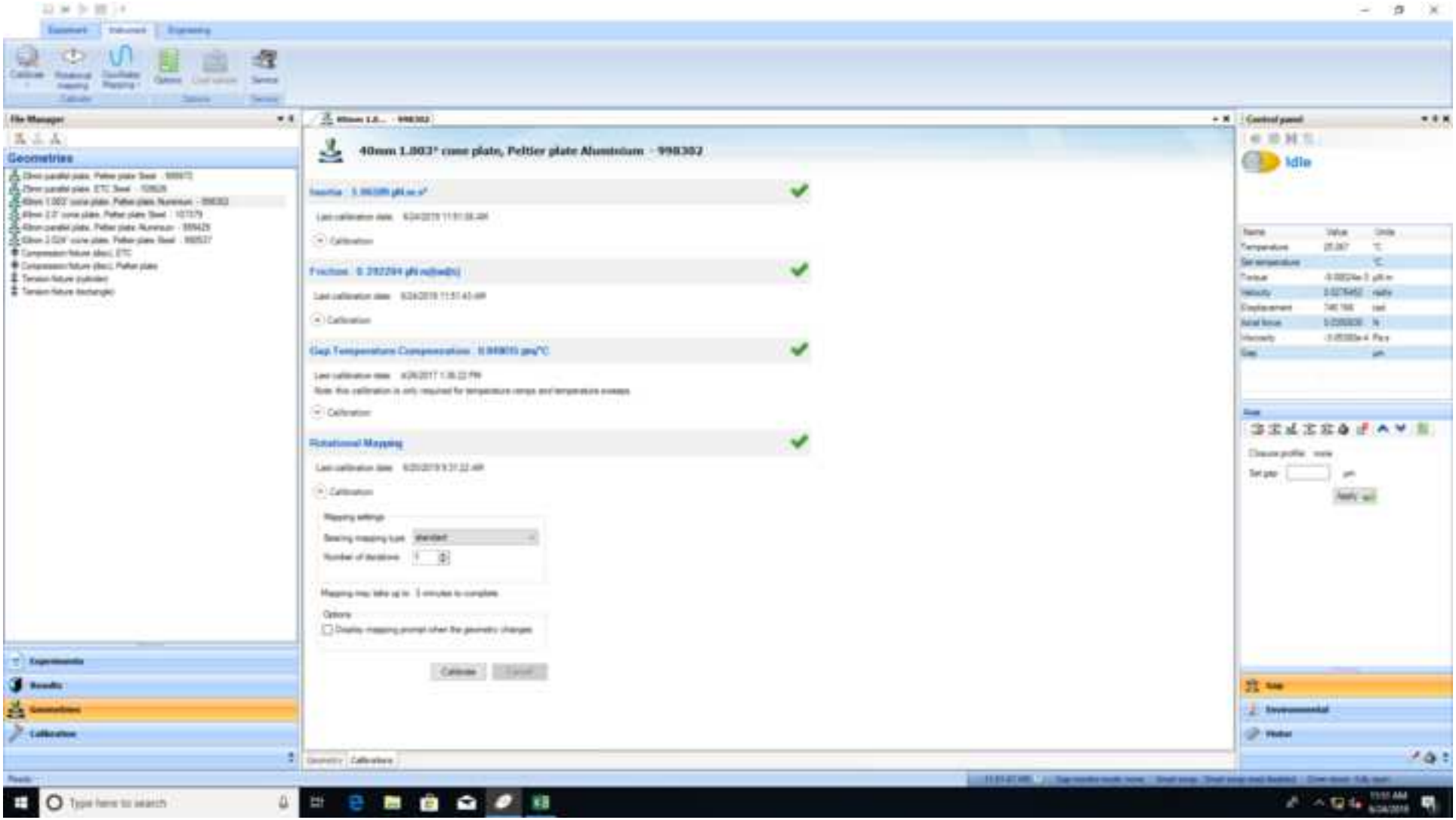

Supplemental File (Figures, Permissions, etc.)
Click here to access/download;Supplemental File (Figures, Permissions, etc.);Supplementary_Figure7.tiff

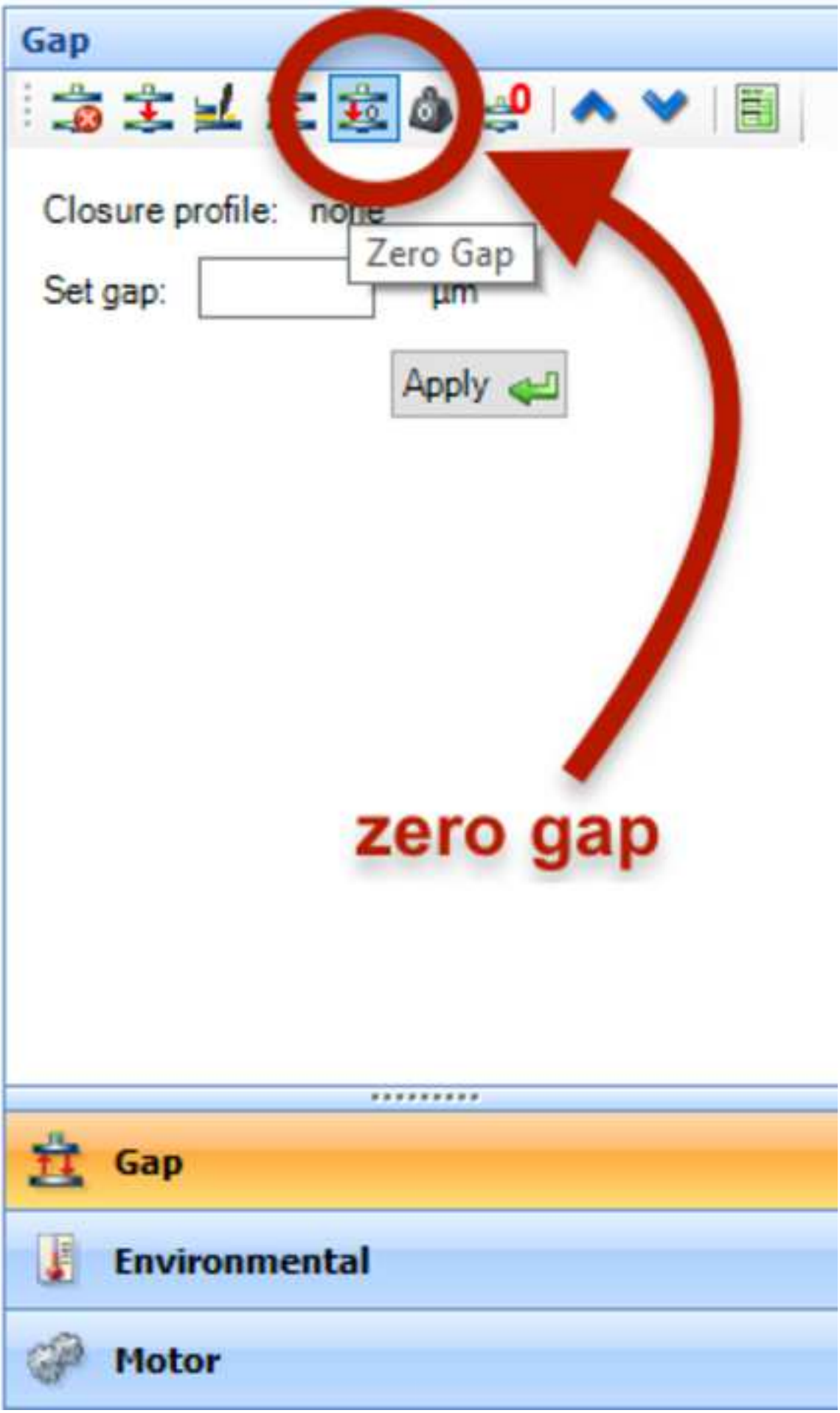

Supplemental File (Figures, Permissions, etc.)
Click here to access/download;Supplemental File (Figures, Permissions, etc.);Supplementary_Figure8.tiff

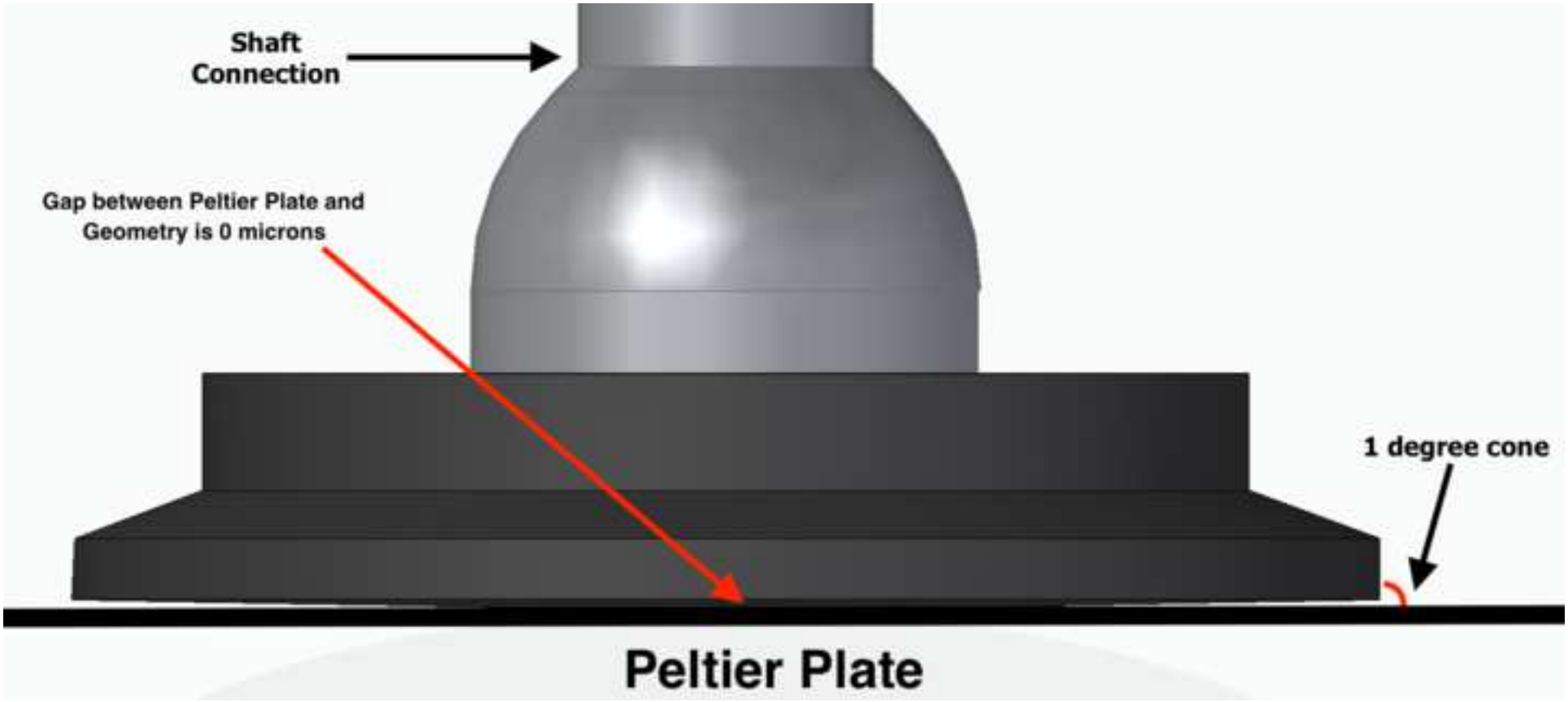

Supplemental File (Figures, Permissions, etc.)
Click here to access/download;Supplemental File (Figures, Permissions, etc.);Supplementary_Figure9.tiff

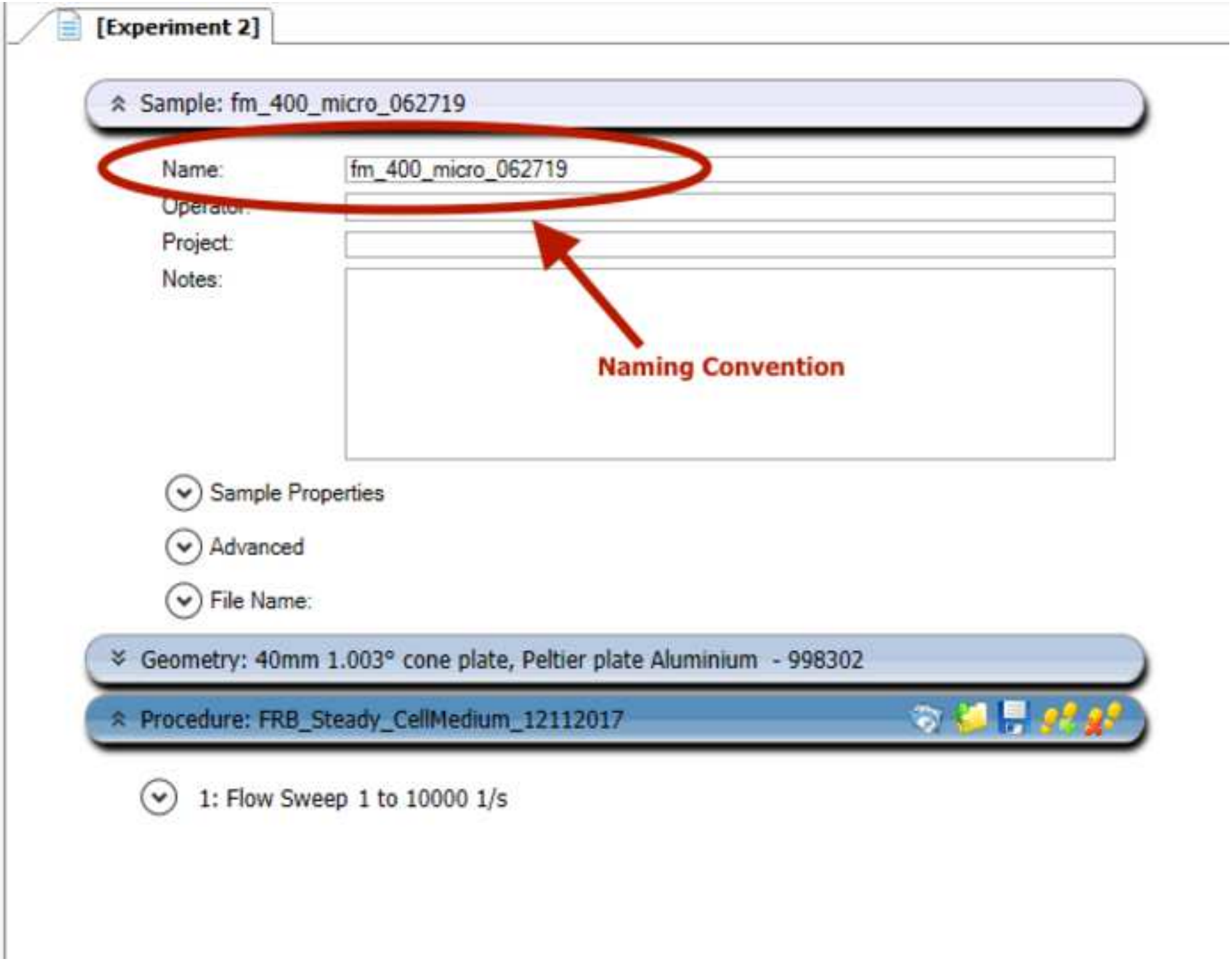

Supplemental File (Figures, Permissions, etc.)
Click here to access/download;Supplemental File (Figures, Permissions, etc.);Supplementary_Figure10.tiff

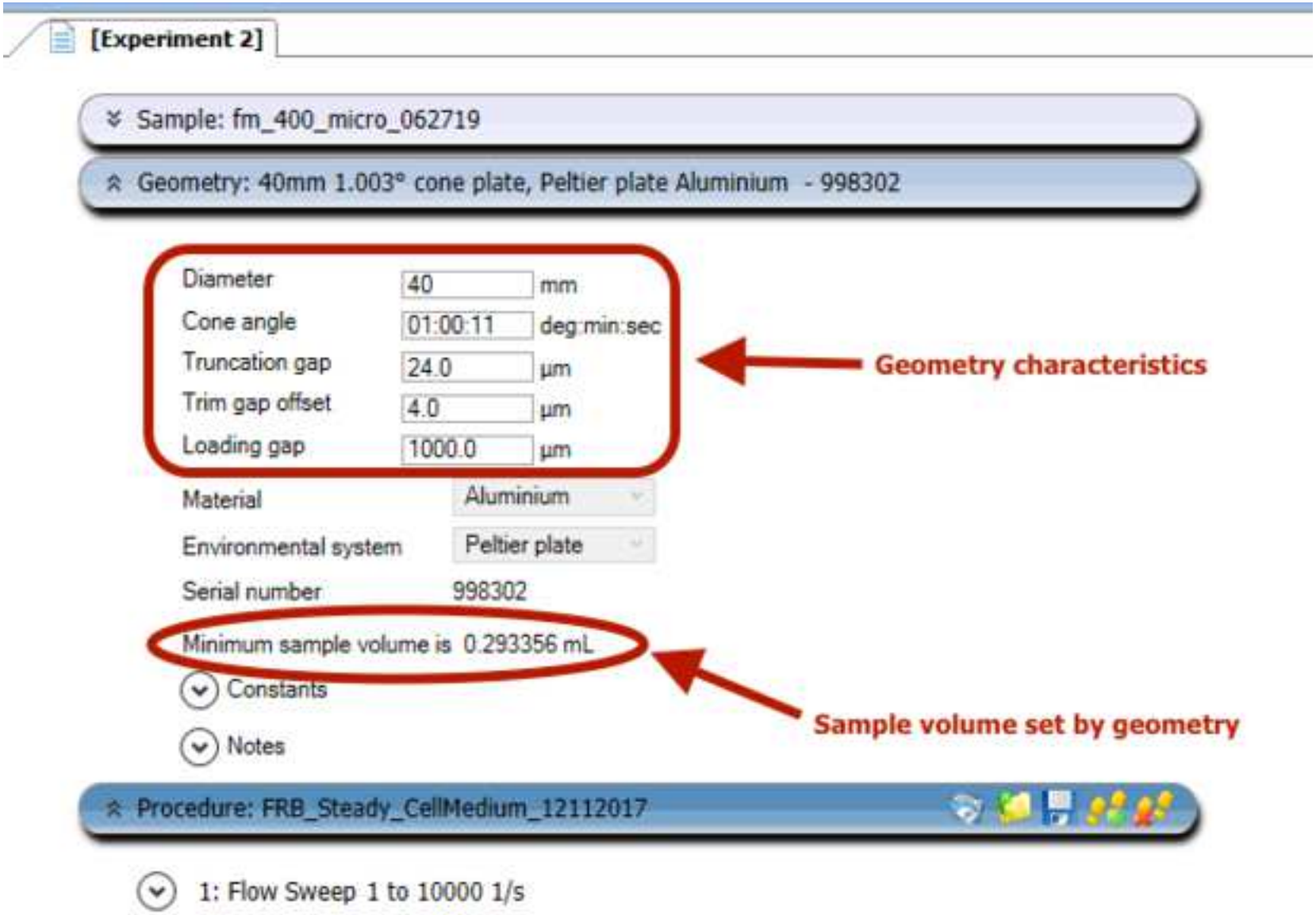

Supplemental File (Figures, Permissions, etc.)

Click here to access/download;Supplemental File (Figures, Permissions, etc.);Supplementary_Figure11.tiff

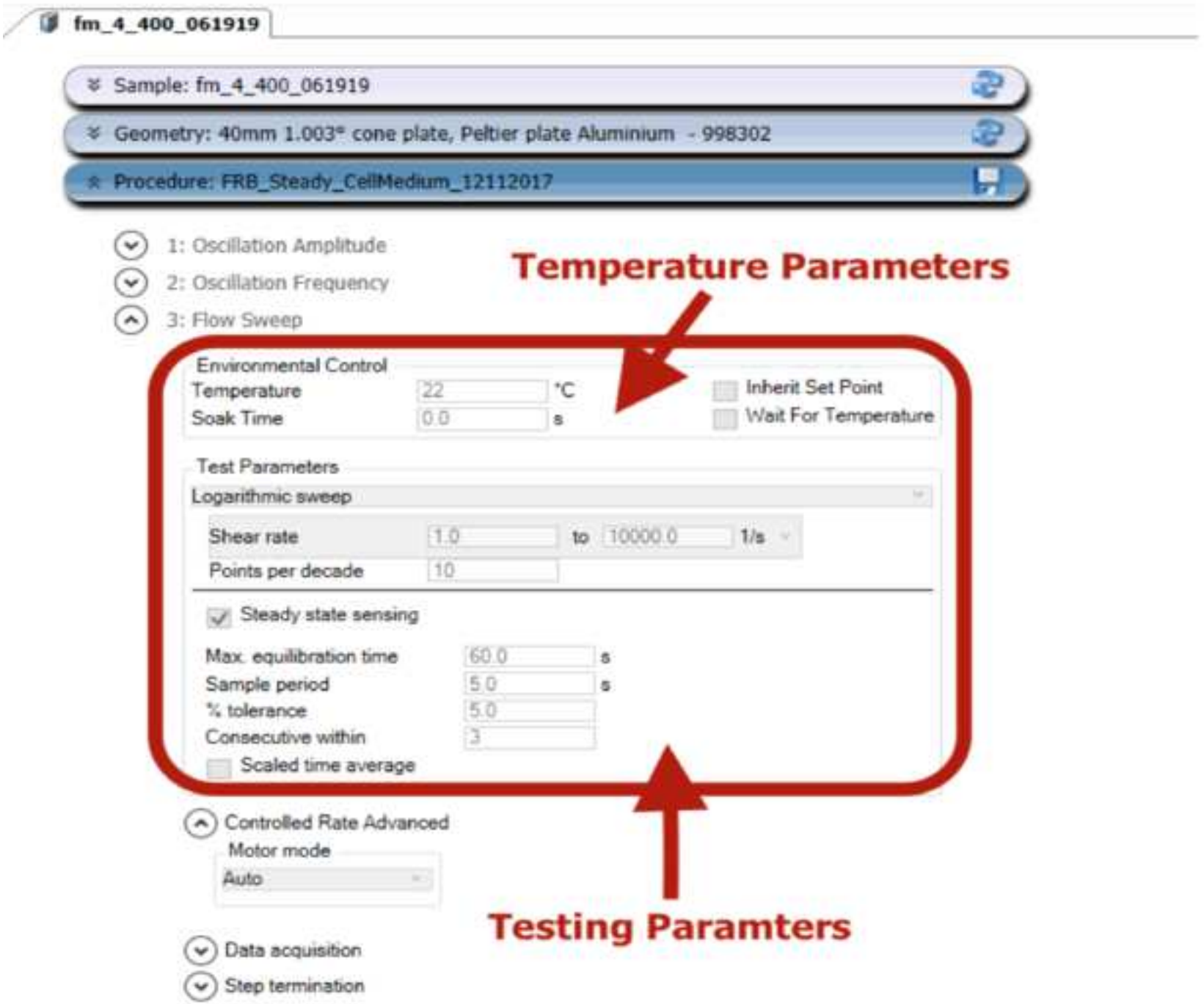

Supplemental File (Figures, Permissions, etc.)
Click here to access/download;Supplemental File (Figures, Permissions, etc.);Supplementary_Figure12.tiff

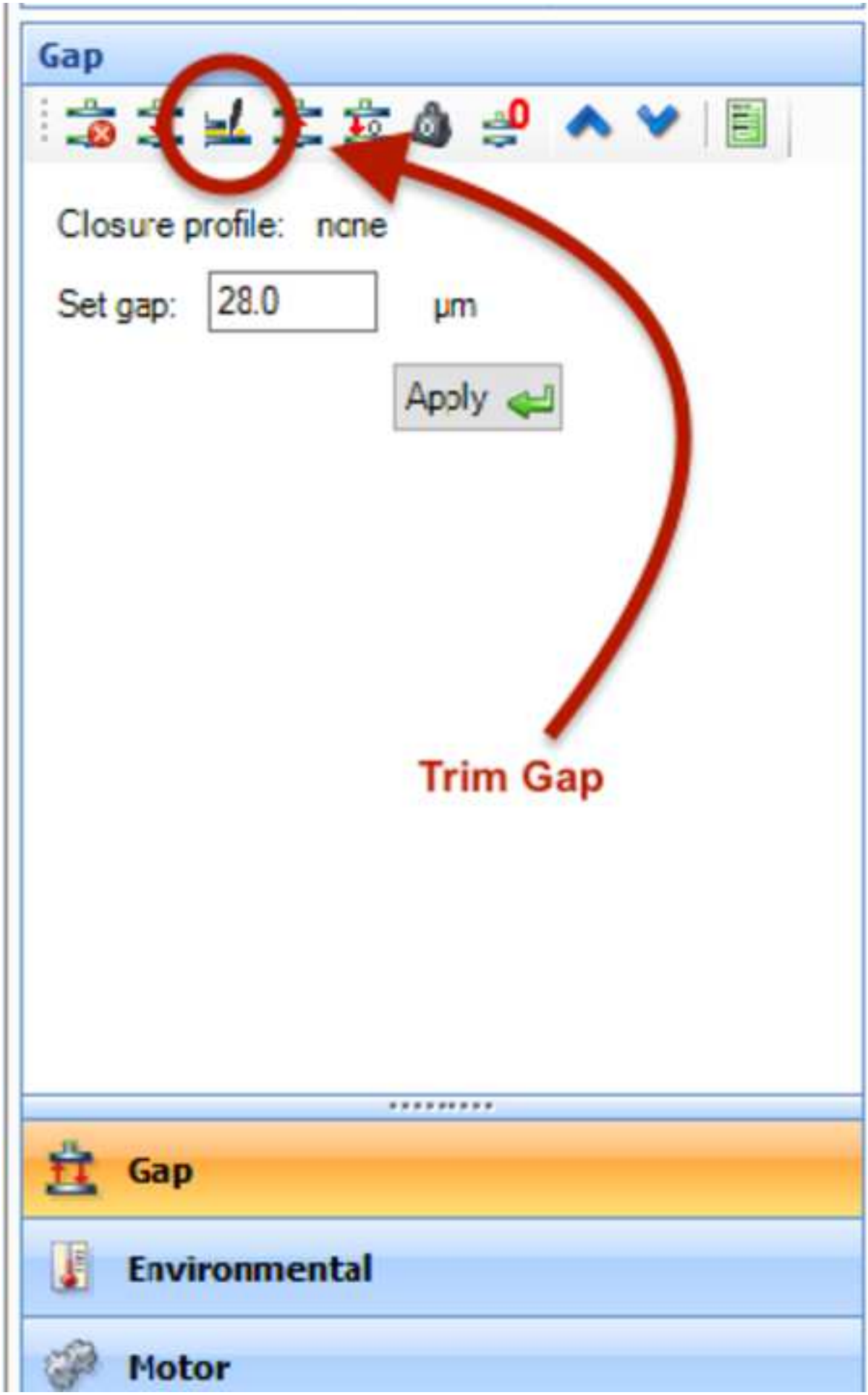

Supplemental File (Figures, Permissions, etc.)

Click here to access/download;Supplemental File (Figures, Permissions, etc.);Supplementary_Figure13.tiff

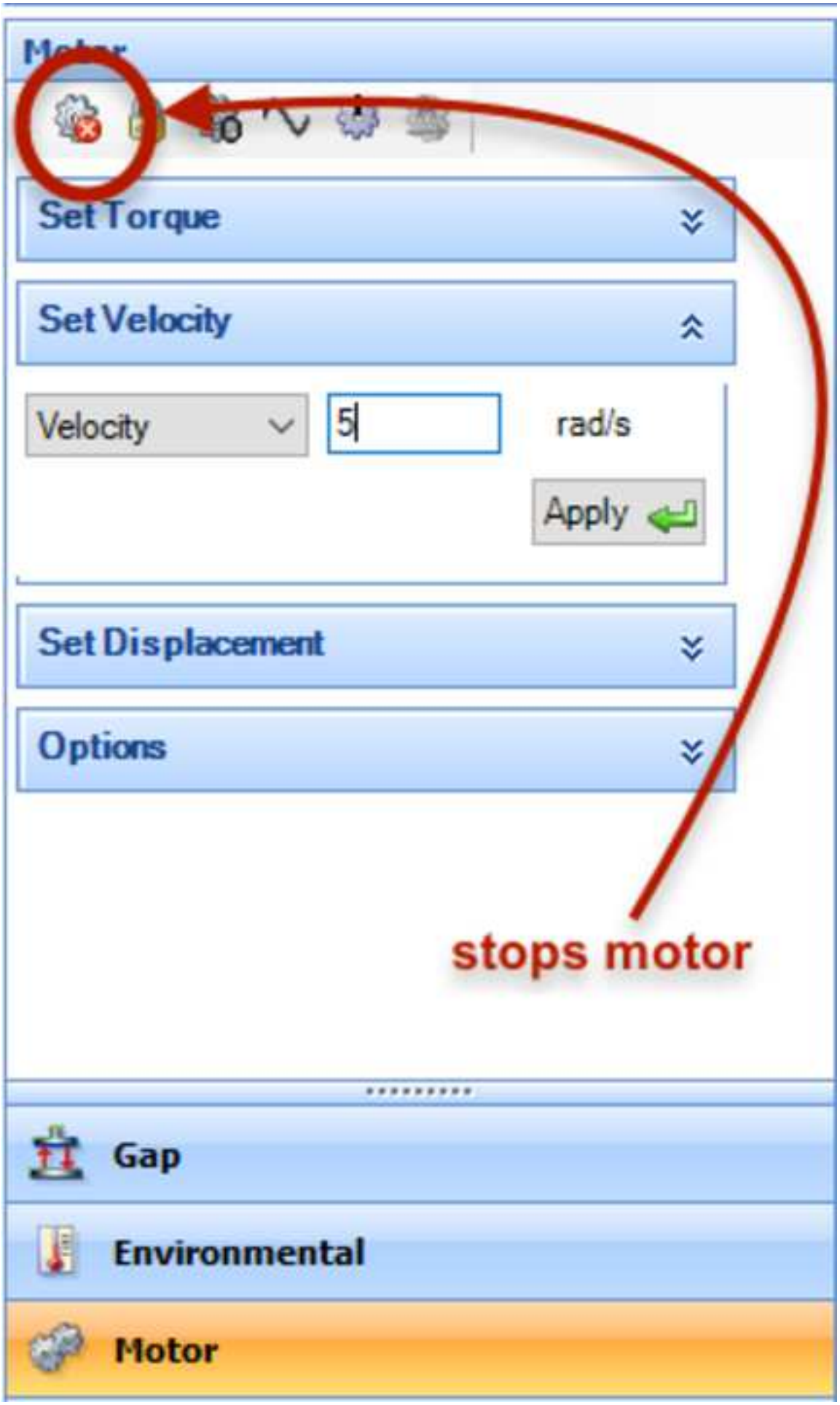

Supplemental File (Figures, Permissions, etc.)

Click here to access/download;Supplemental File (Figures, Permissions, etc.);Supplementary_Figure14.tiff

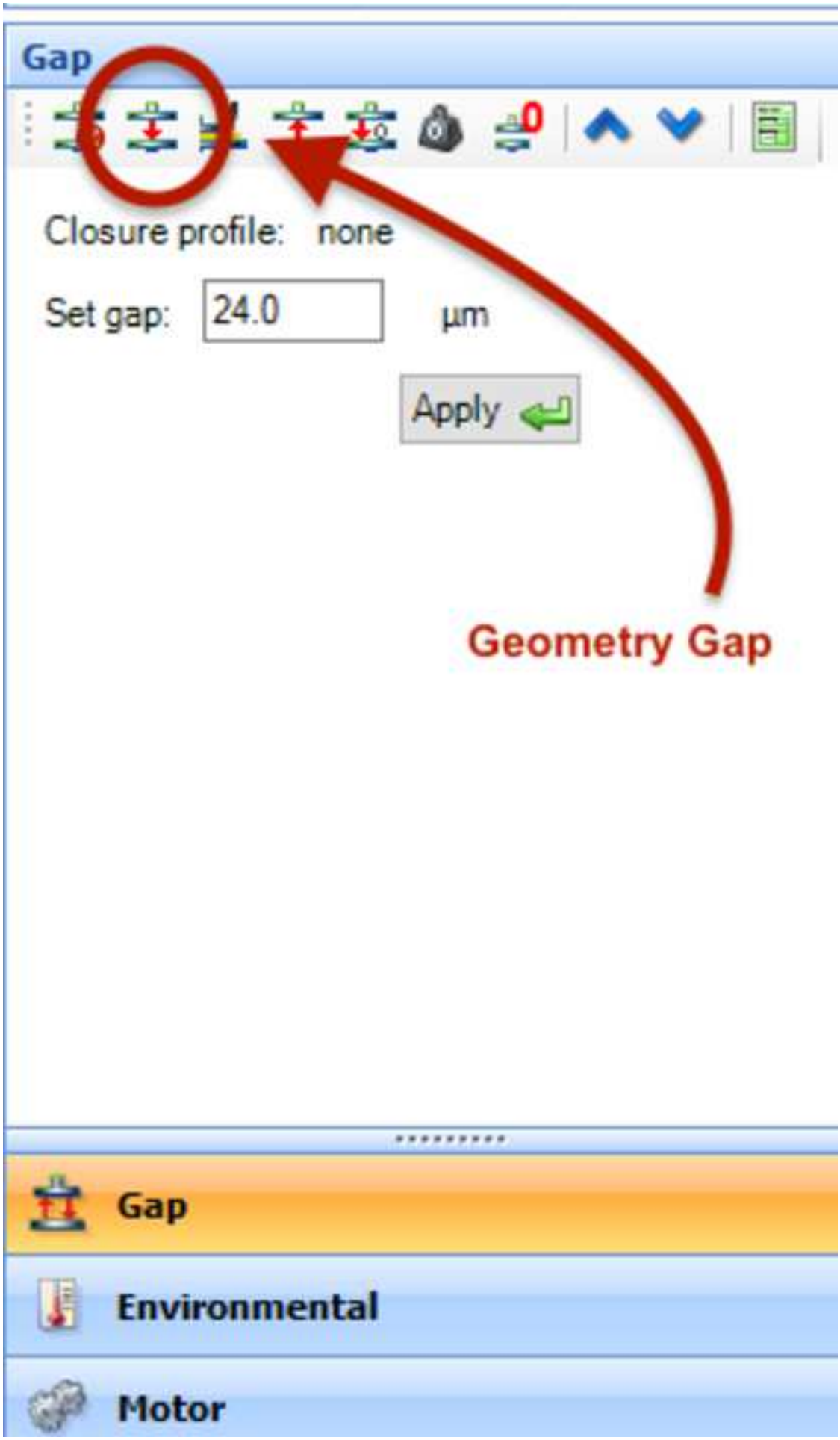

Supplemental File (Figures, Permissions, etc.)

Click here to access/download;Supplemental File (Figures, Permissions, etc.);Supplementary_Figure15.tiff

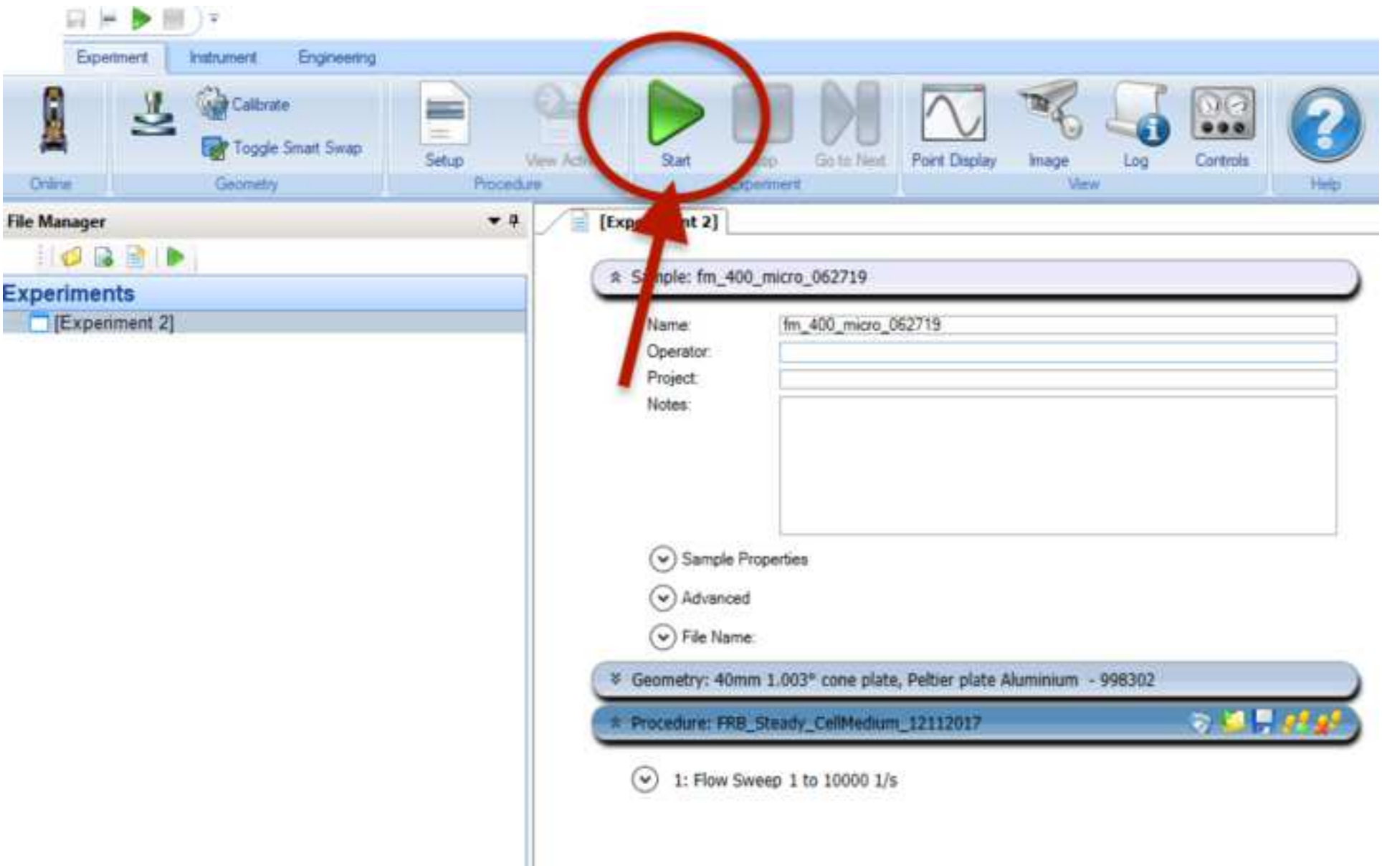

Supplemental File (Figures, Permissions, etc.)

Click here to access/download;Supplemental File (Figures, Permissions, etc.);Supplementary_Figure16.tiff

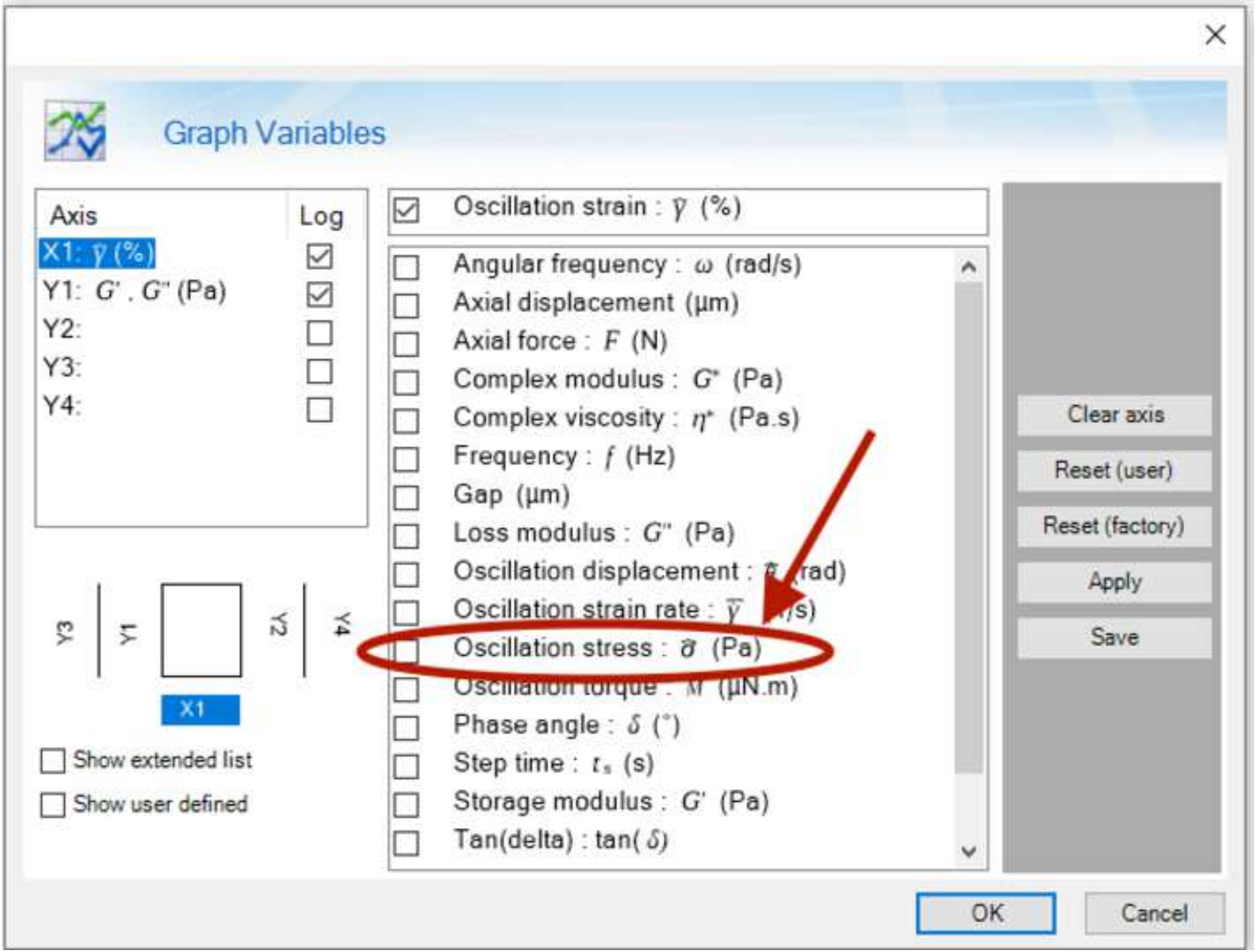

Supplemental File (Figures, Permissions, etc.)

Click here to access/download;Supplemental File (Figures, Permissions, etc.);Supplementary_Figure17.tiff

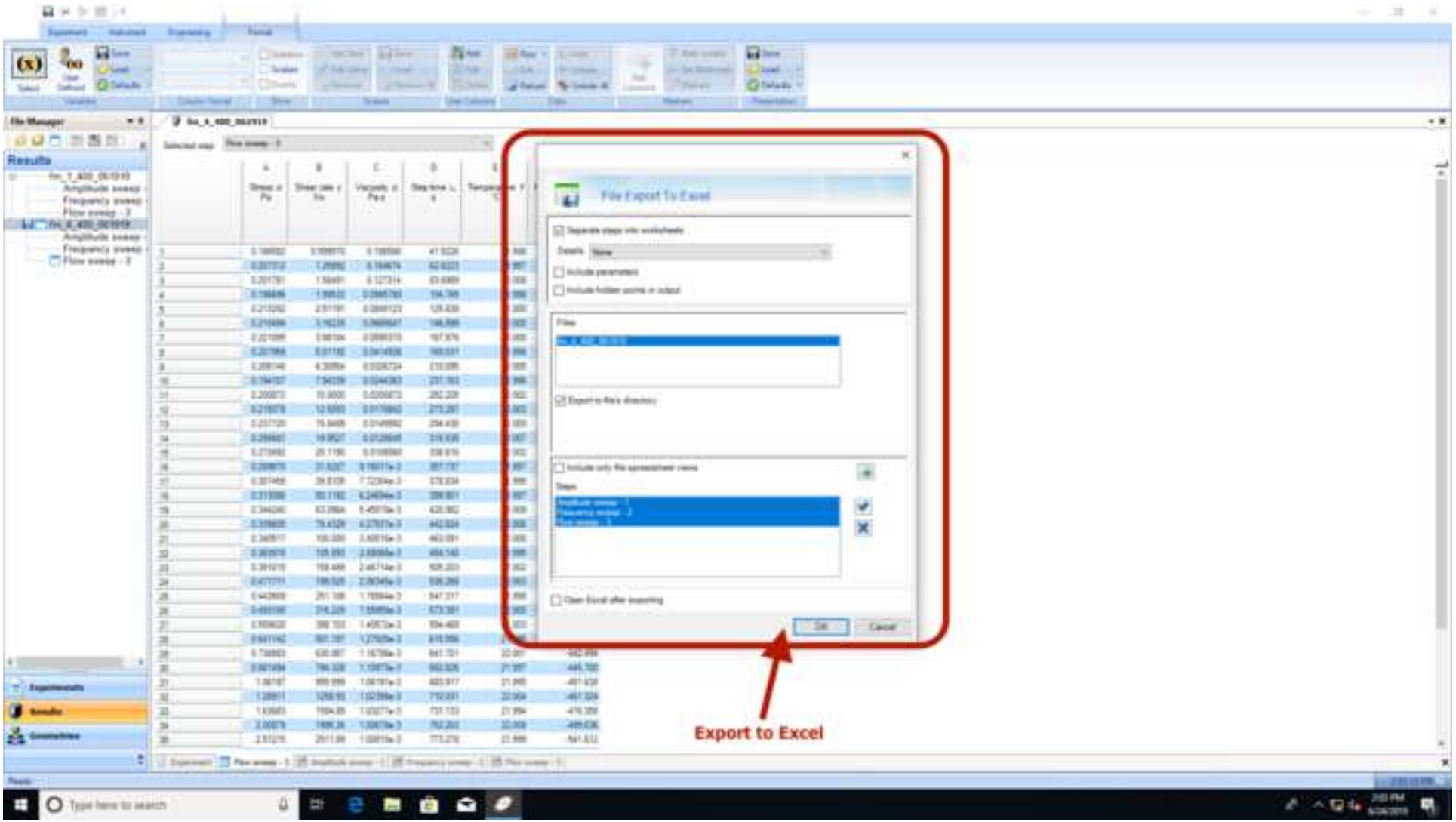

Sample coding file-1 (MATLAB)

Click here to access/download
Supplemental Coding Files
fish_mucus_rheology.m

Sample coding file-2 (MATLAB)

Click here to access/download

Supplemental Coding Files

fm_rheo_amp_sweep.m

Sample coding file-3 (MATLAB)

Click here to access/download

Supplemental Coding Files

fm_rheo_frequency_sweep.m